Since January 2020 Elsevier has created a COVID-19 resource centre with free information in English and Mandarin on the novel coronavirus COVID-19. The COVID-19 resource centre is hosted on Elsevier Connect, the company's public news and information website.

FlatChem 33 (2022) 100377

Contents lists available at ScienceDirect

FlatChem

journal homepage: www.sciencedirect.com/journal/flatchem

2D MXenes for combatting COVID-19 Pandemic: A perspective on latest developments and innovations

Subhasree Panda [a], Kalim Deshmukh [b,*], Chaudhery Mustansar Hussain [c,*], S.K. Khadheer Pasha [a,*]

[a] Functional Nanomaterials and Polymer Nanocomposite Laboratory, Department of Physics, VIT-AP University, Amaravati, Guntur 522501, Andhra Pradesh, India
[b] New Technologies – Research Center, University of West Bohemia, Plzeň 30100, Czech Republic
[c] Department of Chemistry and Environmental Science, New Jersey Institute of Technology, Newark, NJ 07102, USA

ARTICLE INFO

Keywords:
SARS-CoV-2
COVID-19
2D MXene
Antiviral activity
Biocompatibility
Biomedical applications

ABSTRACT

The COVID-19 pandemic has adversely affected the world, causing enormous loss of lives. A greater impact on the economy was also observed worldwide. During the pandemic, the antimicrobial aprons, face masks, sterilizers, sensor processed touch-free sanitizers, and highly effective diagnostic devices having greater sensitivity and selectivity helped to foster the healthcare facilities. Furthermore, the research and development sectors are tackling this emergency with the rapid invention of vaccines and medicines. In this regard, two-dimensional (2D) nanomaterials are greatly explored to combat the extreme severity of the pandemic. Among the nanomaterials, the 2D MXene is a prospective element due to its unique properties like greater surface functionalities, enhanced conductivity, superior hydrophilicity, and excellent photocatalytic and/or photothermal properties. These unique properties of MXene can be utilized to fabricate face masks, PPE kits, face shields, and biomedical instruments like efficient biosensors having greater antiviral activities. MXenes can also cure comorbidities in COVID-19 patients and have high drug loading as well as controlled drug release capacity. Moreover, the remarkable biocompatibility of MXene adds a feather in its cap for diverse biomedical applications. This review briefly explains the different synthesis processes of 2D MXenes, their biocompatibility, cytotoxicity and antiviral features. In addition, this review also discusses the viral cycle of SARS-CoV-2 and its inactivation mechanism using MXene. Finally, various applications of MXene for combatting the COVID-19 pandemic and their future perspectives are discussed.

1. Introduction

The history of pandemics goes long back to Athens in 430B. C. and continued with plague, leprosy, the black death, the Columbian exchange, the Great Plague of London, cholera, Fiji measles, Russian flu, Spanish flu, Asian flu, HIV, SARS, MERS, and the present-day COVID-19 pandemic [1]. First reports of the Severe Acute Respiratory Syndrome Coronavirus 2 (SARS-CoV-2) virus were found in the Hubei Province of China which spread to more than 200 countries in a short period [2]. Taking into account the highly infectious and contagious nature of this virus, World Health Organization (WHO) declared it a public health emergency of international concern (PHEIC) on 30th January 2020 and designated it as the novel coronavirus disease 2019 (COVID-19) [3]. Li et al. [4] implemented a mathematical modeling technique to find the reproduction number R_0 and epidemic doubling time of COVID-19, which indicate the infection rate of the virus. The researchers found a reproductive number of 2.2 (R_0 greater than 1) and an epidemic doubling time of 7.5 days, proving the highly contagious nature of the SARS-CoV-2 virus. The extremely infectious nature of the SARS-CoV-2 disease has made havoc among people, creating greater health impacts and a higher level of mortalities. Not only the health illness but also the hazardous wastes generated during the pandemic has resulted in environmental pollution and greater spreading of the virus [5]. To combat this misery, researchers all over the world set out to discover advanced technologies for medication and vaccine delivery as well as to mitigate the spread of the virus.

The superior physicochemical properties of nanomaterials can be greatly explored to tackle this emergency. The extraordinary quantum

* Corresponding authors.
E-mail addresses: deshmukh@ntc.zcu.cz (K. Deshmukh), chaudhery.m.hussain@njit.edu (C. Mustansar Hussain), khadheerbasha@gmail.com (S.K. Khadheer Pasha).

https://doi.org/10.1016/j.flatc.2022.100377
Received 5 March 2022; Received in revised form 15 April 2022; Accepted 27 April 2022
Available online 30 April 2022

mechanical properties of the nanomaterials can be utilized to build sophisticated biomedical instrumentations like photosterilizers, touch-free sanitizers, contact tracing tools, etc. [6]. The production rate and durability of biomedical equipment like PPE kits, face shields, respirators, etc. can be improved by the readily synthesized efficient nanomaterials. Highly sensitive, rapid, and accurate detection of the viral infection by improved clinical methods like serological tests can be done by using the rapid sensing and conducting properties of the 2D nanomaterials [7]. The antipathogenic features of the nanomaterials can be utilized to inactivate the SARS-CoV-2 viruses by generation of photocatalytic/ photothermal/ photodynamic therapy-induced reactive oxygen species. The coating of nanomaterials on the face masks and PPE kits can filtrate and inactivate the virus by their superior antiviral properties [7]. The high surface area of the 2D nanomaterials can be used for a greater drug loading and the nano range of the materials can provide point-specific drug delivery to internal organs like COVID-19 affected alveoli [7]. The nanomaterials can be designed to activate/inactivate the immune system, thereby providing efficient vaccine delivery and prevention of cytokine release syndrome (CRS) [7]. The nanomaterials can also be used as potent biosensors for the detection of SARS-CoV-2 viruses and their related biomarkers (Fig. 1) [7].

Since the emergence of the pandemic, the development in finding a suitable vaccine has been progressing with a greater effort. The COVID-19 vaccines mainly rely on the administration of antigens based on the mRNA, DNA, recombinant proteins, viral vectors, and attenuated or inactivated viruses, focusing mostly on the inactivation of viral S proteins [8]. However, the delivery of these therapeutics is hindered due to their vulnerability to enzymatic degradation and impermeability to cell membranes [9]. The polymeric, inorganic, or lipid-based nanoparticles can be used as encapsulation to avoid these issues and to provide effective non-invasive (nasal, oral, transdermal, pulmonary, etc.) methods for drug and vaccine delivery [9]. For improving the efficacy of vaccines and considering the mutation of the viruses, the nanomaterials can be functionalized with different types of molecules targeting specific pathogens [7]. Nanomaterials with specific and non-specific mechanisms of antiviral action can be administered to inhibit viral activity [10]. The nanomaterials having a specific mechanism of action, target particular surface receptors or ligands of the virus; whereas the nanomaterials having a non-specific mechanism of action inhibit any part of the virion [10]. The nanomaterials can modify the function of accessory proteins (ORF7a), spike glycoproteins (S), envelope (E), and membrane (M) proteins, etc. of the virus [10]. In some cases the nanomaterials releases various ions and therapeutics that pass through the envelope to disrupt virus protein machinery by dysfunctioning the proteases like NSP3 (pappain-like protease), NSP5 (main protease), NSP7, NSP8, NSP9 (RNA replicase), NSP10, NSP13 (helicase), etc. (Fig. 2a) [10]. The nanomaterials also release the inhibitors of ACE2 and TMPRSS2 to inhibit the entry complex formation. If the virus breaks the barrier and enters the host cell, the nanomaterials provide the second line of defense by the disruption of virion endosomal acidification, intracellular vesicle formation for RNA transcription, blocking of crown shape molecular pores, packaging, and exocytosis of new virions, etc. (Fig. 2b) [10].

Among the nanomaterials, the 2D MXene can play a great role to combat the pandemic due to its superior antiviral activities, photocatalytic and photothermal properties, greater conductivity, excellent surface structure, superior sensing, and electromagnetic shielding properties, etc. The superior antiviral properties of MXenes can be utilized for coating face masks, PPE kits, face shields, etc. making them less infectious and reusable [11]. This can also help for environmental remediation by the less exposure to disposable plastics made out of face masks and PPE kits, etc [12]. The enhanced photocatalytic and photothermal activities of MXenes can help to inactivate the virus [13,14], as well as the superior sensing activities can help to build efficient biosensors that can detect the COVID-19 virus and other biomarkers in the case of patients having comorbidities [15]. The greater drug loading and point-specific drug release capacity of MXene can be utilized for delivering the drug in remote parts of the internal organs of COVID-19 patients [16]. Along with these, the greater biocompatibility and lesser cytotoxicity of MXene reduce the risk of poisoning as seen in the case of other advanced materials [17].

Many advanced nanomaterials have been explored to date for the detection and inactivation of the SARS-CoV-2 virus, but they also have lots of limitations. Seo et al. [18] fabricated a graphene-based field-effect transistor (FET) biosensor by coating a specific antibody of SARS-CoV-2 spike protein. The COVID-19 FET sensor successfully detected the antigen protein as well as measured the viral load in culture medium and clinical samples. However, the device lacks resilience and requires pre-processing of the virus sample, due to the comparatively low signal-to-noise ratio of the graphene sensing material. The MXene-graphene FET sensor fabricated by Li et al. [19] eliminated the loopholes of graphene-based FET sensor for the detection of the SARS-CoV-2 virus. The authors used a virus-sensing transduction material (VSTM) consisting of both MXene and graphene. They found that the enhanced performance is due to the hydrophilic surface functional groups and accordion-like structure of MXene that provides greater active sites for virus adsorption. The zero band gap of graphene also restricts its

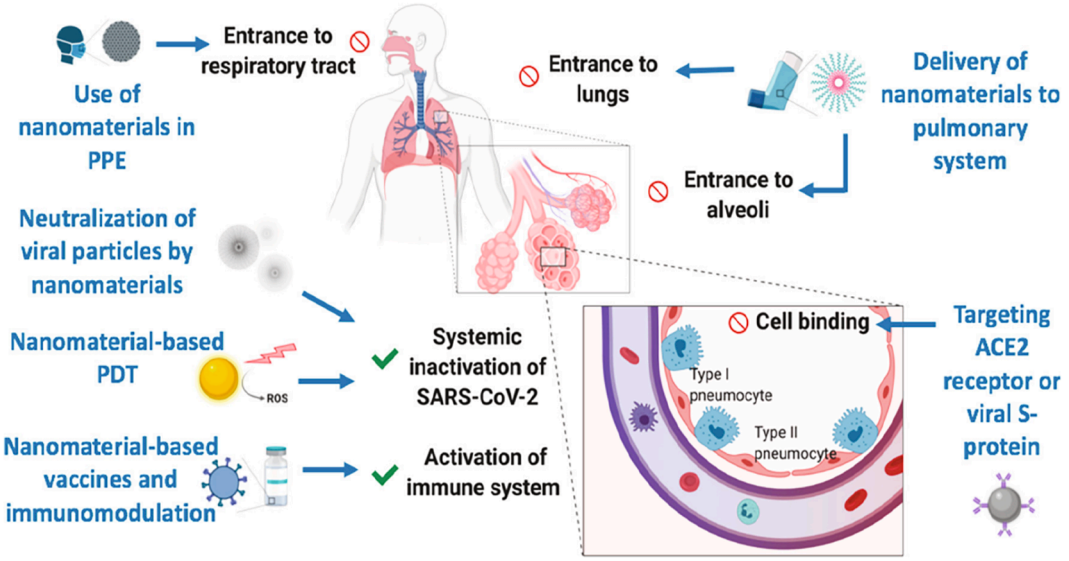

Fig. 1. Prospective applications of nanomaterials in combatting COVID-19 pandemic. Adapted from Ref. [7], Copyright 2020, American Chemical Society.

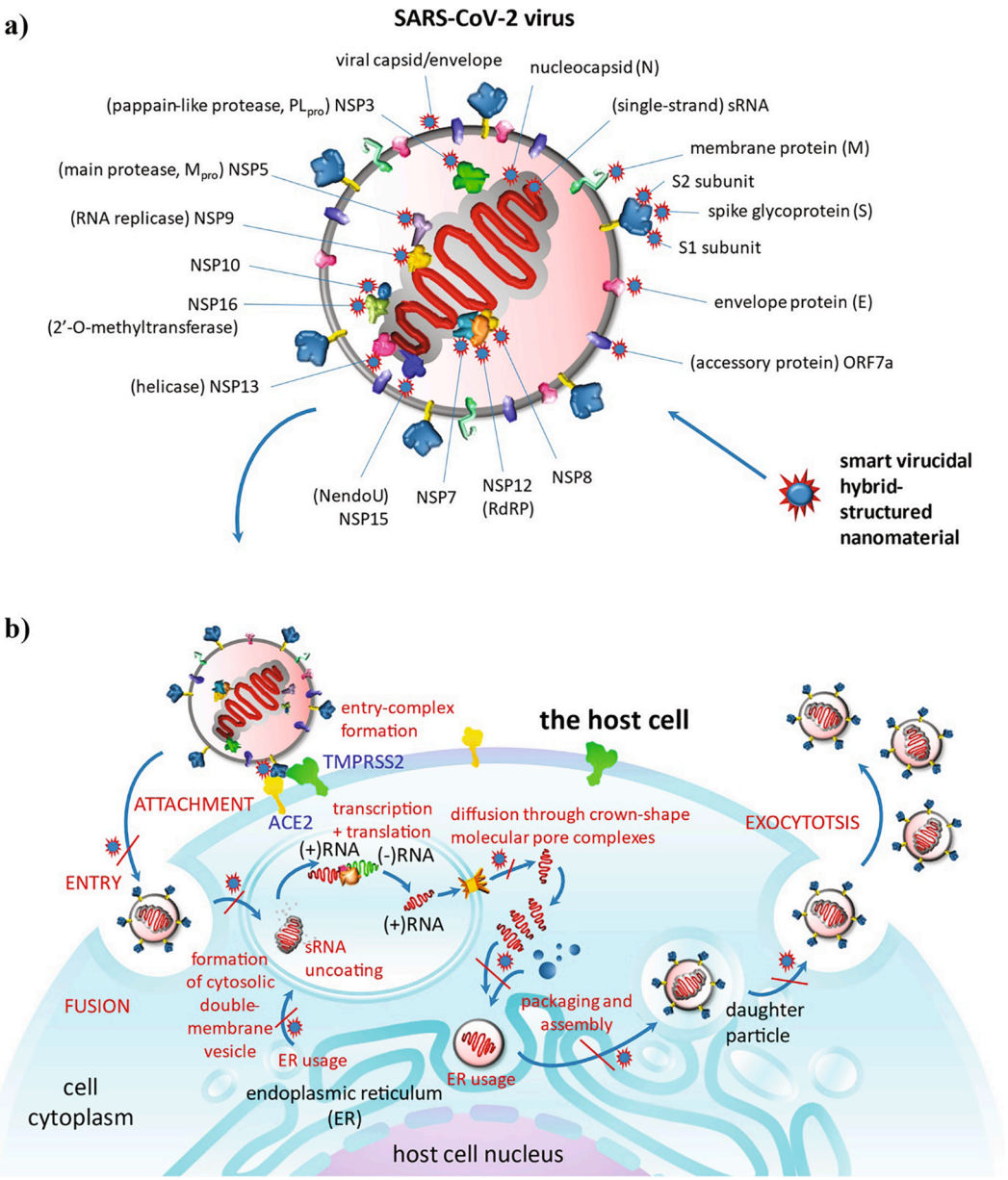

Fig. 2. Representation of inactivation mechanism of the virus using nanomaterials, (a) inside the host cell, (b) outside the host cell. Adapted from Ref. [10], Copyright 2021, American Chemical Society.

application as a biosensor for the fast and accurate detection of viruses, whereas the metallic nature of MXene provides a greater bandgap for sensing [20]. On the other hand, transition metal dichalcogenides (TMDs) have a greater band gap, but the high electrical noise limits their sensing application [21]. MXene-based biosensors provide extremely low noise and ultrahigh signal-ro noise ratio, which is beneficial for rapid sensing activity [22]. MXenes have reported a greater adsorption capacity than graphene and a faster rate of removal than carbon nanotubes [23]. This property can be beneficial for faster adsorption and removal of virus, cytokines, and other biomarkers from the body of COVID-19 patients. Although MXenes have made tremendous progress in biomedical instrumentations and antimicrobial applications, their properties are less explored in the field of antiviral applications. Hence, this review deeply studies the MXene antiviral properties as well as the perspectives of using MXene as a sword to win the battle against the COVID-19 pandemic. Table 1 summarizes different properties of MXenes that can be useful for prevention and diagnosis of Covid-19 virus.

Table 1
Summary of prospective prevention and diagnosis of COVID-19 using 2D MXene.

Sl. No.	MXene properties	MXene based prevention and diagnosis of COVID-19	Ref.
1	Photocatalytic	Virus inactivation	[13]
2	Photothermal	Virus inactivation	[14]
3	Anti-inflammatory	Vaccine and drug delivery	[17]
4	Adsorption	Removal of contaminants	[33]
5	Amino acid adsorption	Trapping of virus	[72]
6	Modification of spike protein	Hindrance of virus life cycle	[73]
7	Histocompatibility	Reduced cytotoxicity	[82]
8	Photoacoustic imaging	Diagnosis of internal organs	[84]
9	Urea Adsorption	Dialyzer	[107]
10	Porous structure	Fabrication of face masks	[112]
11	Sensing	Biosensor (detection of biomarkers)	[123]
12	Viscoelasticity	3D printed biomedical instruments	[129]

2. 2D MXenes

MXenes are the large family of 2D transition metal carbides, nitrides, or carbonitrides, discovered in 2011 by Gogosti et al. [24]. They have a chemical formula of $M_{n+1}X_nT_x$ (n = 1 to 4), where M is an early transition metal (Ti, V, Cr, Nb, Mo, etc.), X is carbon and/or nitrogen, and T_x indicates the surface termination groups like –F, –OH, -O, etc [15,25]. $Ti_3C_2T_x$, Ti_2CT_x, Ti_2NT_x, Ti_3CNT_x, V_2CT_x, Nb_2CT_x, $Cr_2TiC_2T_x$, $Ti_3SiC_2T_x$, $Mo_4VC_4T_x$, etc. are some of the examples of synthesized MXenes, from which the $Ti_3C_2T_x$ is the most explored one [26]. Till now more than 30 MXenes have been synthesized and more than 100 MXene stoichiometries have been predicted by simulations, making them one of the largest families of 2D materials [17]. The double transition metal MXenes are comprised of two transition metal atoms as compared to mono transition metal MXenes [27]. The double transition metal MXenes are of two types, i.e. solid solutions having a random distribution of transition metals in the M sites of the 2D structure ($(Ti, Nb)_2CT_x$, $(Ti, V)_2CT_x$, etc.) and ordered forms having in-plane ($Mo_{4/3}Y_{2/3}CT_x$, $Mo_{4/3}Sc_{2/3}CT_x$)/out-of-plane ($Mo_2TiC_2T_x$, $Mo_2Ti_2C_3T_x$, $Cr_2TiC_2T_x$, etc.) ordered structures (Fig. 3) [28]. MXenes name is derived from graphene due to their similar properties [29]. They have hexagonal layered structures similar to their parent MAX phases, in which the X layers are interleaved between the M layers with functional groups attached to the surface structure [30,31]. The scanning electron microscopy (SEM) images confirm the lamellar structure of the MXenes [32]. The bonding between the M and A elements is purely metallic, whereas the M−X bond combines the characteristics of covalent, ionic, and metallic bonds, but the M−A bonds are quite unstable as compared to the M−X bonds [29]. They have excellent physicochemical properties, which lead to their wide range of applications in energy storage devices, gas sensing, catalysis, electromagnetic interference shielding, and biomedical fields [13,31,33,34]. Fig. 4 gives a representation of MXene applications in various sectors [31].

3. Synthesis of 2D MXenes

MXenes can be synthesized by both top-down and bottom-up methods [28]. In the top-down methods, the A layers are etched out from the 3D MAX or non-MAX phase precursors resulting in the 2D layered MXenes. The strong metallic bond between the M and A layers of the MAX phase resists its exfoliation by mechanical shearing methods [29]. The high-temperature treatment can exfoliate the A layers but the synthesized MXenes lose their layered structure due to recrystallization of the material [29]. Therefore, the exfoliation of A layers can be achieved by using chemical etching methods like hydrofluoric acid (HF) etching, alkali etching, acid/fluoride salt etching, molten salt etching, and electrochemical etching, etc. followed by sonication or intercalation with organic bases or cations [35]. Intercalants like dimethyl sulfoxide (DMSO) [36], urea [37], isopropylamine [38], hydrazine monohydrate [39], tetrabutylammonium hydroxide (TBAOH) [40], tetramethylammonium hydroxide (TMAOH) [41], aryl diazonium salts [42], etc. are commonly used for increasing the interlayer distance, thereby resulting in the efficient exfoliation of MXenes. Also, the cations like Al^{3+}, Mg^{2+}, Li^+, Na^+, K^+, NH_4^+, etc. are intercalated spontaneously or electrochemically to achieve the exfoliated MXenes [43]. Fig. 5 illustrates etching, intercalation and delamination processes of MXenes [31].

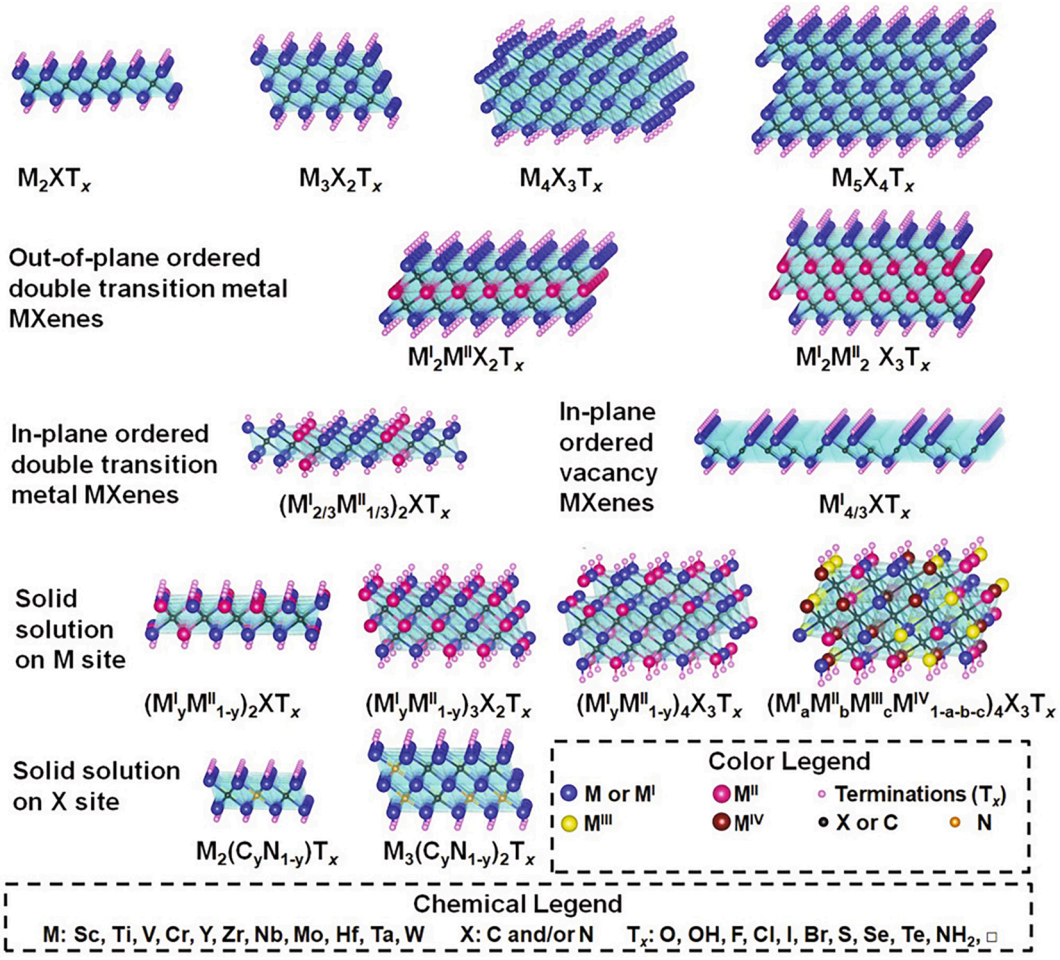

Fig. 3. Classification of single and double transition metal MXenes. Reproduced with permission from Ref. [28], Copyright 2021, John Wiley and Sons.

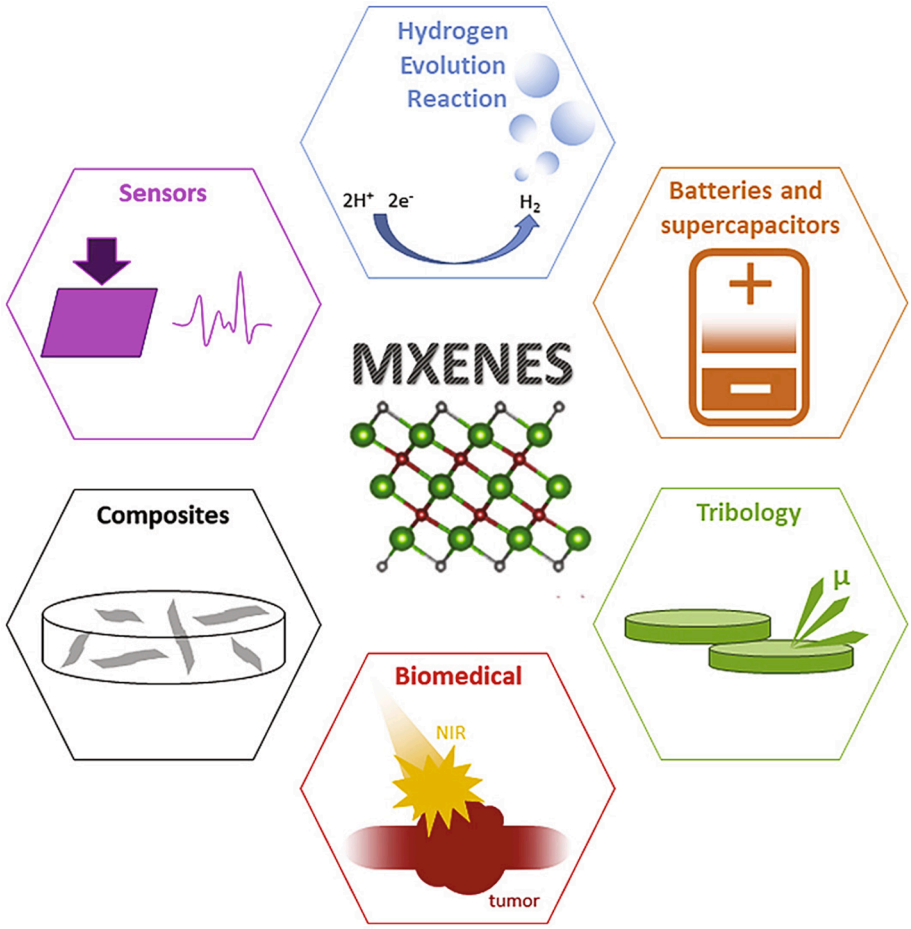

Fig. 4. Representation of MXene applications in various sectors. Reproduced with permission from Ref. [31], Copyright 2019, Elsevier.

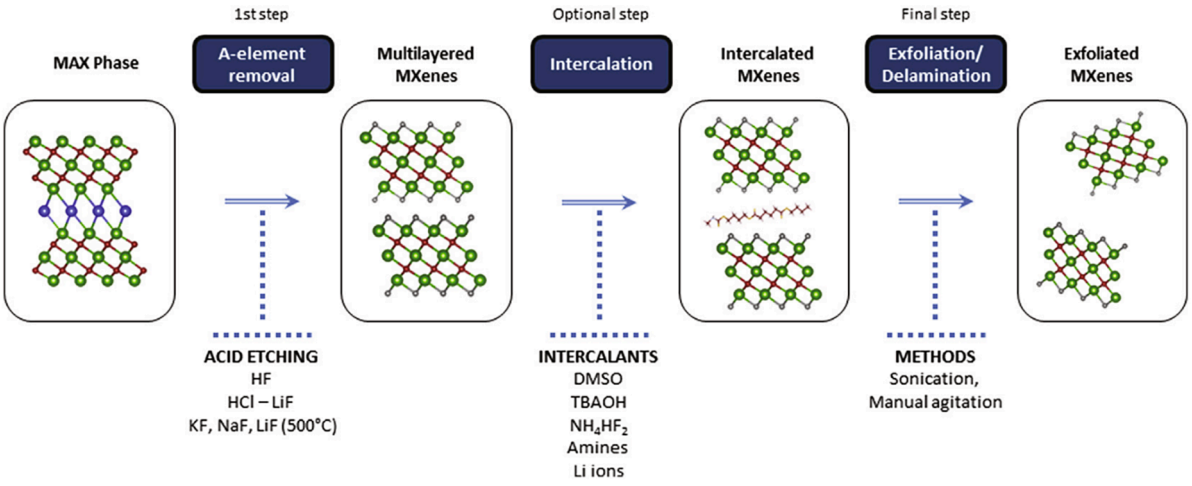

Fig. 5. Illustration of MXene etching process followed by the intercalation and delamination. Reproduced with permission from Ref. [31], Copyright 2019, Elsevier.

Naguib et al. [44] synthesized the first MXene Ti_3C_2 by etching the A layers of the Ti_3AlC_2 MAX phase in 50% HF acid at RT for a duration of 2hr. This mechanism can be illustrated as follows;

$$M_{n+1}AX_n + 3HF \rightarrow M_{n+1}X_n(s) + AF_3 + 1.5H_2(g) \quad (1)$$

$$M_{n+1}X_n(s) + 2HF \rightarrow M_{n+1}X_nF_2 + H_2(g) \quad (2)$$

Although MXenes were tremendously etched out using HF, the hazardous and toxic nature of the acid discard it as an efficient etchant for MXene synthesis [45]. Hence, more effective green synthesis methods were followed by the HF etching. Ghidiu et al. [46] etched Ti_3AlC_2 MAX phase by the in situ formed HF using the less aggressive acid/ fluoride salt mixture of HCl and LiF. Subsequently, other MXenes like Mo_2CT_x [47], V_2CT_x [48], Ti_3CNT_x [49], etc. were synthesized using different combinations of acids (HCl or H_2SO_4) and fluoride salts (KF, NaF, CsF, CaF_2, etc.). Simultaneous etching and delamination of the MXenes were obtained due to the Li^+ ion intercalation within the interlayers [50].

$$HCl\ (aq)\ +\ LiF\ (aq) \rightarrow HF\ (aq)\ +\ LiCl\ (aq) \quad (3)$$

MXenes obtained by this method were having a larger interlayer gap and minimum crystal defects as compared to the HF etched MXenes [51]. Halim and coworkers synthesized Ti_3C_2 MXene films by etching the Al layers of sputter-deposited epitaxial Ti_3AlC_2 films using NH_4HF_2 as an etchant [52]. These etching processes result in the negative surface functional groups terminations on the MXene surface like -F, –OH, -O, etc., which is responsible for the formation of their stable colloidal solutions [53]. The structure and properties of the synthesized MXenes largely vary depending upon the atmospheric moisture and temperature, exposure to UV radiations, delaminating agents, etching time, etching solution, etc. [50]. For example, the increase in temperature helps in accelerating the exfoliation of MXenes but it leads to the enhancement of oxidation too [50]. Similarly, higher atomic number and larger bond energy MAX phases require high concentration etchants and greater etching time [29]. Conversely, as compared to the top-down methods, in the bottom-up methods, MXenes are synthesized by the combination of their corresponding atoms/molecules. Xu et al. [54] first used this strategy to synthesize the Mo_2C MXene by the chemical vapor deposition (CVD) method. Followed by this, other bottom-up methods like template method [55], plasma-enhanced pulsed laser deposition method (PEPLD) [56], etc. were discovered for the synthesis of MXenes. Fig. 6 describes the evolution of MXene synthesis methods over the past decade [57].

4. A brief story on SARS-CoV-2 and its viral mechanism

To study the antiviral properties of MXenes, it is essential to deeply understand the mechanism of virus infection. Coronaviruses are a group of encapsulated RNA viruses that have an approximate spherical structure with a dimension of 60–140 nm [58]. The club-like spike proteins emanating from the surface of the virion resemble the structure of a solar corona, giving it the name coronavirus [59]. These viruses cause both acute and chronic illnesses in humans and animals. Among the six coronavirus species discovered so far, four of them cause common flu, whereas the Severe Acute Respiratory Syndrome Coronavirus (SARS-CoV) and the Middle East Respiratory Syndrome Coronavirus (MERS-CoV) are fatal [60,61]. The SARS-CoV-2 is named so by considering the similarity of the virus with the previous SARS-CoV outbreak [62]. The genome sequence of the SARS-CoV-2 virus shows similarities with the previous strains of SARS-CoV and MERS-CoV, but has a greater transmission rate. For example, the sequence analysis showed similarities of more than 80% with SARS-CoV and more than 50% with MERS-CoV [63]. The human cell entry receptors for both the SARS-CoV-2 and SARS-CoV variants are the same angiotensin-converting enzyme II (ACE2) protein [64].

To develop drugs and vaccines for the diagnosis of the COVID-19 disease, it is essential to know the genomic sequence of the SARS-CoV-2 virus. The Global Initiative on Sharing All Influenza Data (GISAID), a platform that provides open access genomic sequence data of the influenza viruses has reported 8 clades of the SARS-CoV-2 genomes, among which the mutated clades GR, S, and GH are found in most of the countries worldwide as compared to other clades having wild type genomes [65]. Researchers have reported the missense mutation in the SARS-CoV-2 spike protein D614G as the predominant clade of viral infection in most countries, due to its greater binding affinity to ACE2 receptors, efficient cellular entry, and minimal antibody interactions [66–68]. This mutation has been found mostly in the GH and GR clades of the SARS-CoV-2 virus, making it more promising for the faster spreading of infection [17].

The crystal structure study of the C-terminal domain of the SARS-CoV-2 spike S protein reveals the binding affinity of the virus to human ACE2 receptors [69]. The attachment of the spike S protein of the virus to the ACE2 receptor leads the Transmembrane serine protease 2 (TMPRSS2) to facilitate protease activity for cell entry [70]. As binding of the virus is a key factor for the initiation of infection, inhibition of this mechanism can lead to the reduction of viral infection to a greater extent. Treatments using recombinant ACE2, monoclonal antibodies, TMPRSS2 inhibitors, etc. have been widely recommended to impede viral binding [71]. Followed by the cell entry, the internalization of the virus occurs by endocytosis. The low pH of the endosome results in the uncoating of the viral genome and release into the cytoplasm for further viral RNA and protein synthesis, resulting in the assembly of viral infections (Fig. 7) [7]. Several antiviral therapies have been administered to date for the regulation of viral RNA production, cytokine release, and blood coagulation [71].

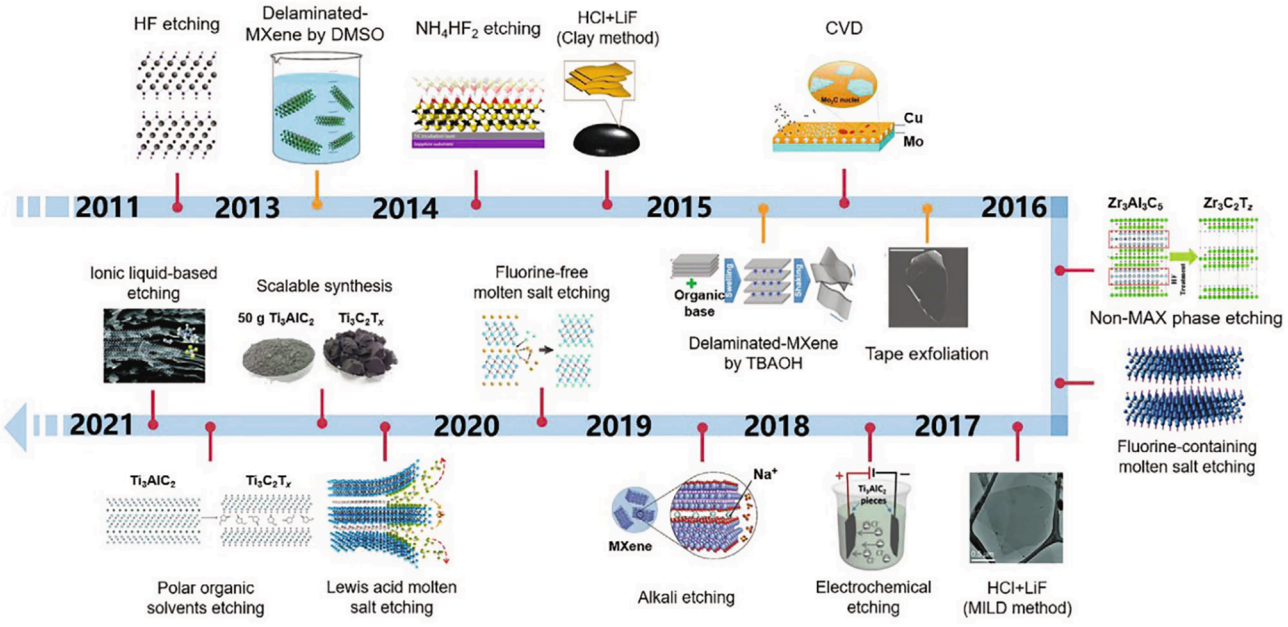

Fig. 6. Evolution of different synthesis processes of MXenes. Reproduced with permission from Ref. [57], Copyright 2021, John Wiley and Sons.

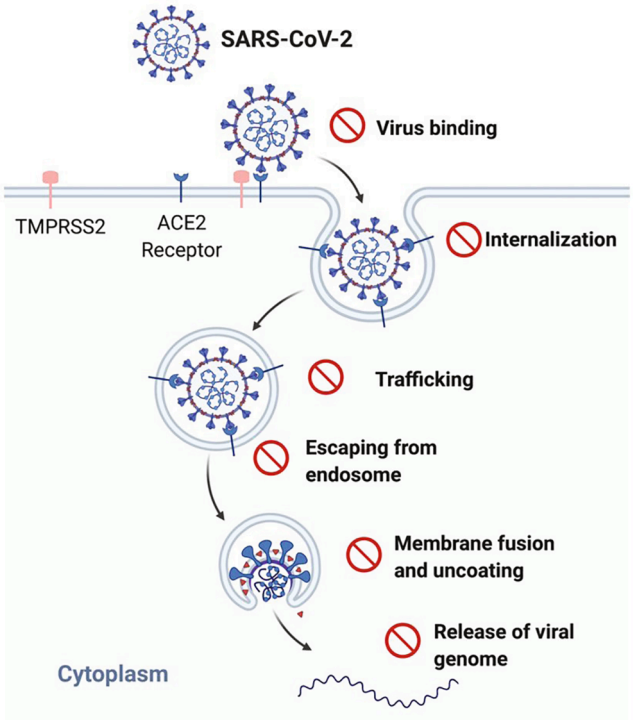

Fig. 7. Schematic illustrating the binding of viral S protein to ACE2 receptor followed by internalization and release of the viral genome into the cytoplasm. Adapted from Ref. [7], Copyright 2020, American Chemical Society.

5. MXenes as antiviral material

5.1. Antiviral activities

The superior antiviral properties of MXenes impart a great promise for its biomedical applications. The hydrophilic MXene contains a superior negative surface functional groups, which when applied as a coating on face masks, PPE kits, etc. traps the viruses and either inactivates or kills them by interacting with the outer spike proteins. The strong adsorption between the MXene surface and the amino acids contained in the peplomers results in the trapping of the virus onto the surface of MXene and its subsequent inactivation [11,72]. Unal et al. [17] delineated the antiviral properties of the most explored $Ti_3C_2T_x$ MXene by treating them with the SARS-CoV-2 (GR, GH, S, and other clades) infected Vero E6 cells culture. The qRT-PCR results of the viral GR clade infected supernatant reported a 99 % reduction of the viral copy numbers for the dilution till 1: 3,125. Whereas, no significant viral inhibition was observed for the other clades (Fig. 8A-D) [17]. These findings emphasized the importance of considering the viral genotypes and mutations while evaluating the antiviral efficacy of the nanomaterials and other candidate molecules. A remarkable improvement in the viability of the virus-infected Vero E6 cells was observed in the presence of MXene with minimal cytotoxicity (Fig. 8E, F) [17]. The authors also studied the antiviral activities of $Ti_3C_2T_x$, $Ta_4C_3T_x$, $Mo_2Ti_2C_3T_x$, and $Nb_4C_3T_x$ MXenes by exposing them to the GR clade of the SARS-CoV-2 and found out $Ti_3C_2T_x$ to be the most potent antiviral among all of them [17]. $Ti_3C_2T_x$ exhibited 99% viral copy numbers reduction at a concentration of 0.32 μg/ml (1: 3,125 dilution), whereas $Mo_2Ti_2C_3T_x$ reported a reduction of 95% viral copy numbers at a concentration of 100 μg/ml (Fig. 9B) [17]. $Nb_4C_3T_x$ and $Ta_4C_3T_x$ did not show any significant antiviral activity either with GR and GH clades having D614G missense mutation or with other clades (Fig. 9A, C, E, F) [17]. The researchers also subjected the culture to TiO_2 nanoparticles to prove that, it's the $Ti_3C_2T_x$ MXene that exhibits antiviral activity and not the Ti particles (Fig. 9D) [17]. Ghasemy et al. [73] experimented with the interaction of Mo_2C, Ti_2C, and Mn_2C MXene nanosheets with the spike proteins of the SARS-CoV-2 virus and found out that MXenes not only adsorb the spike proteins effectively but also modify their secondary structure. This hinders their interaction with the angiotensin-converting enzyme 2 (ACE2) receptors of human cells, which are responsible for the COVID-19 infection. The authors also observed a greater potential of Mn_2C MXene for inhibiting the infection as compared to other MXenes [73].

Ghasemy et al. [73] studied the antiviral activities of MXenes by doing in-silico molecular dynamics simulations. They exposed the nanosheets of Mo_2C, Ti_2C, and Mn_2C to the spike proteins of the SARS-CoV-2 and analyzed the interaction of MXene exposed spike proteins with ACE2 receptors by molecular docking analysis. They reported docking energy of −351.7 kJ/mol for the interaction of spike proteins and ACE2 receptors without any exposure to MXene. The re-docking analysis of MXene treated spike proteins and ACE2 receptors exhibited lesser interaction energies of −312.7, −271, and −253 kJ/mol for Mo_2C, Ti_2C, and Mn_2C MXenes, respectively. The authors attributed the lesser energy to the distorted structure of MXene treated spike proteins that hindered the interaction with ACE2 receptors. As reported in the literature, to diminish the stability of spike proteins, it is required to increase the turn, bend, and coil while decreasing the α-helices and β-sheets of their secondary structure. Among the three MXenes, Mn_2C reported the lowest docking energy revealing the highest portion of the turn, bend, and coil (Fig. 10a). In accordance with the configurational analysis, the energy analysis of the interaction between MXenes and spike proteins reported the highest interaction energy for Mn_2C MXene with an energy level of −290 kJ/mol [73]. The interaction energies for Mn and Ti-based MXenes were favoured by van der Waals forces, whereas the interaction energies for Mo_2C MXenes were dominated by electrostatic forces (Fig. 10b). The entropy analysis of the interlinkage between spike protein and deformed spike protein with ACE2 receptors exhibited a lower entropy for the MXene treated spike proteins/ACE2 systems. This decrease in entropy revealed greater stability and suppression in the infection rate of the spike protein/ACE2 system. Mn_2C MXene, having the greatest interaction energy reported the lowest entropy followed by Ti_2C and Mo_2C, respectively (Fig. 10c). The decrease in the compactness of spike proteins led to a reduction in stability and weaker interaction with ACE2 receptors. The compactness was measured by the difference in the initial and final radius of gyration. All MXenes gave rise to a reduction in the radius of gyration, but Mn_2C exhibited the most negative value of −0.3 (Fig. 10d) [73]. This is in line with the impact of MXene on the secondary structures of spike proteins that reduce the number of active sites by structural molding. Fig. 10h and i show the conformation of the interaction between ACE2 and spike protein before and after the exposure to Mo_2C MXene. Furthermore, the average number of hydrogen bonds (H-bonds) for the Mn_2C exposed spike protein/ACE2 system was the lowest with an average number of 8, which confirms the lesser interactions of MXene treated spike proteins (Fig. 10e). In addition to this, the RDF analysis reported a lesser distribution of the MXene-mediated spike proteins in the vicinity of ACE2 receptors, revealing a lesser probability of infection (Fig. 10f). Moreover, the RDF analysis of the MXene/spike protein system reported the highest RDF value of 3.4 for the Mn_2C/spike protein interaction, showing a greater affinity of Mn_2C MXene to the spike proteins, compared to Ti_2C and Mo_2C MXenes (Fig. 10g). The greater performance of Mn_2C over Mo_2C can be attributed to the smaller size of Mn atoms that offer a greater contact area with the spike proteins and contributes to a greater deformation. Despite the fact that Ti atoms are smaller than Mn atoms, the metallic nature of Mn_2C promotes greater electron donation, resulting in the profound deformation of spike proteins [74].

5.2. Photo-induced activities

Studies have shown a relative inhibition of the COVID-19 virus activities with increasing temperature [75]. The elevated temperature

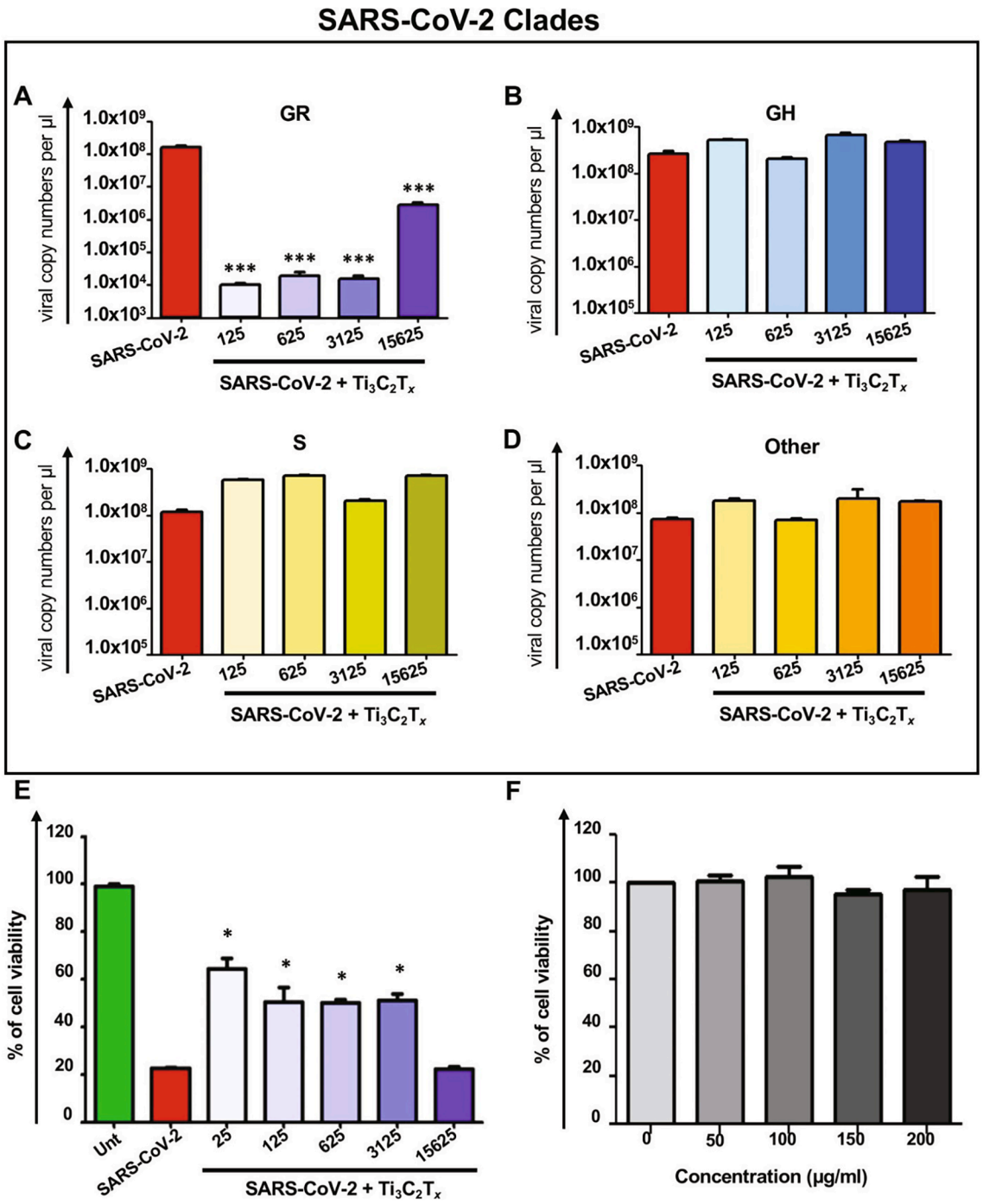

Fig. 8. Schematic illustrating, the viral inhibition of the (A) GR, (B) GH, (C) S, and (D) other clades of the SARS-CoV-2 virus by treatment with $Ti_3C_2T_x$ MXene in variable dilution after a duration of 48 hr. (E) Viability of the SARS-CoV-2 infected Vero E6 cells in different dilutions of $Ti_3C_2T_x$ MXene after a duration of 48 hr. (F) Measurement of cytotoxicity on the Vero E6 cells after exposure of MXene in different concentrations after a duration of 4 hr. Reproduced with permission from Ref. [17], Copyright 2021, Elsevier.

disintegrates the genomic sequence of the virus, resulting in its inactivation [76]. With the increase in temperature, the disintegration becomes faster. The efficient photothermal properties of MXenes can help to kill the virus by facile optical to thermal conversion methods [14]. This property can be beneficial for the self-disinfection of PPEs, masks, gloves, and other protective units. Li et al. reported 100% internal light to heat conversion efficiency for the Ti_3C_2 MXene, thus enabling MXene a suitable nanomaterial for antiviral applications [77]. Lin et al. observed superior photothermal stability and greater photothermal conversion efficiency of ~44.7% for the Ta_4C_3 MXene nanosheets [78]. Along with this, the photocatalytic properties of MXenes can inactivate the virus by interacting with its spike proteins [13]. Thus, efficient photo-sterilizers with greater performance can be fabricated by using these properties of MXenes. Photodynamic therapy can be used for the excitation of photosensitizers by radiating a light source in the presence of oxygen to produce reactive oxygen species (ROS) leading to the damage of the SARS-CoV-2 virus structure [79]. Zhang et al. [80] studied the photo-induced properties of the Mo_2C nanospheres in the near-infrared region and found its extraordinary photothermal and photodynamic therapy efficiency along with CT imaging and

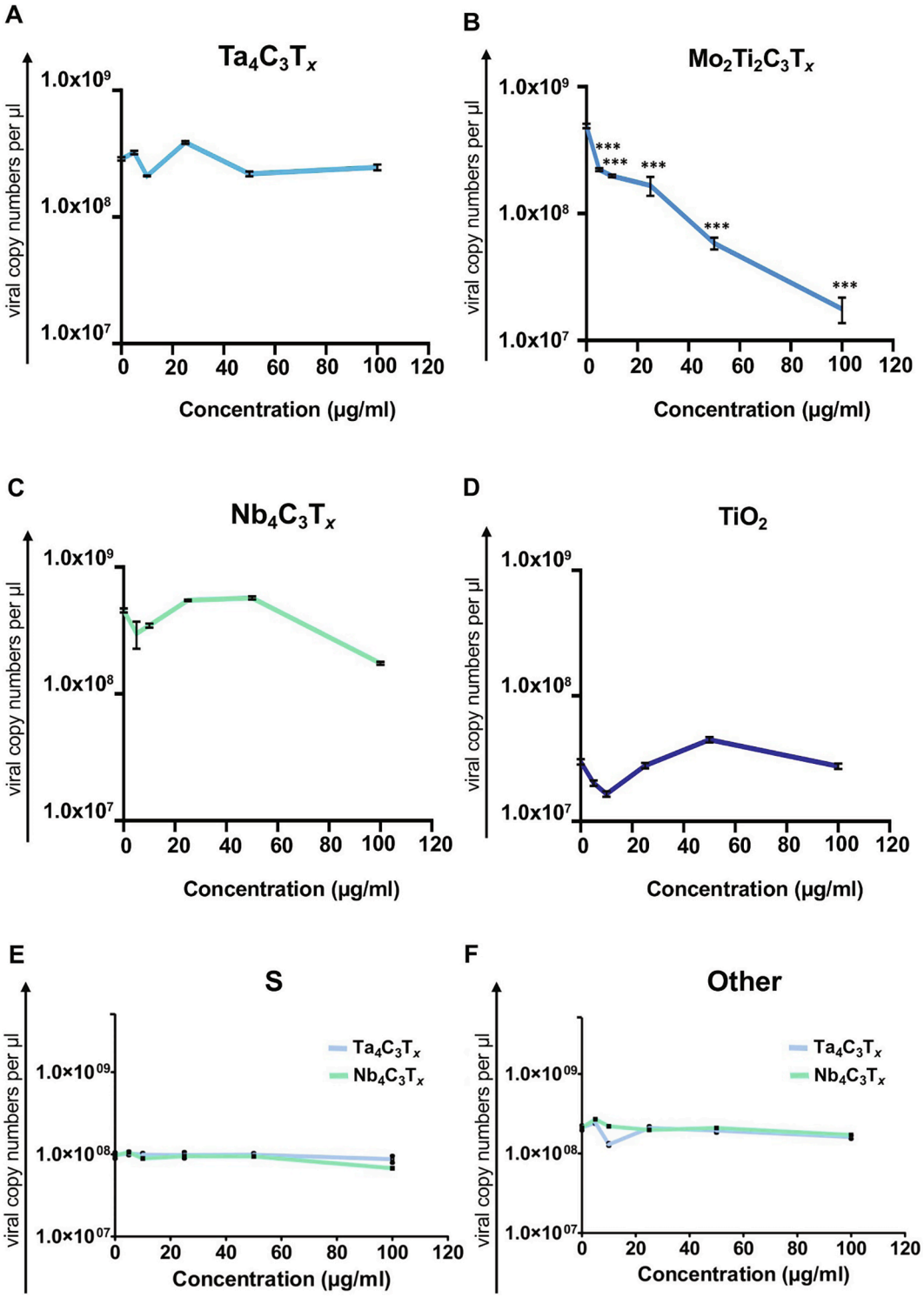

Fig. 9. Graphs indicating the change in viral copy numbers of the (A) $Ta_4C_3T_x$, (B) $Mo_2Ti_2C_3T_x$, (C) $Nb_4C_3T_x$ MXenes, and (D) TiO_2 treated Vero E6 cells, infected with SARS-CoV-2 GR clade. (E, F) Change in viral copy numbers of the $Ta_4C_3T_x$ and $Nb_4C_3T_x$ treated Vero E6 cells, infected with SARS-CoV-2 S and other clades, as observed in the qRT-PCR test. Reproduced with permission from Ref. [17], Copyright 2021, Elsevier.

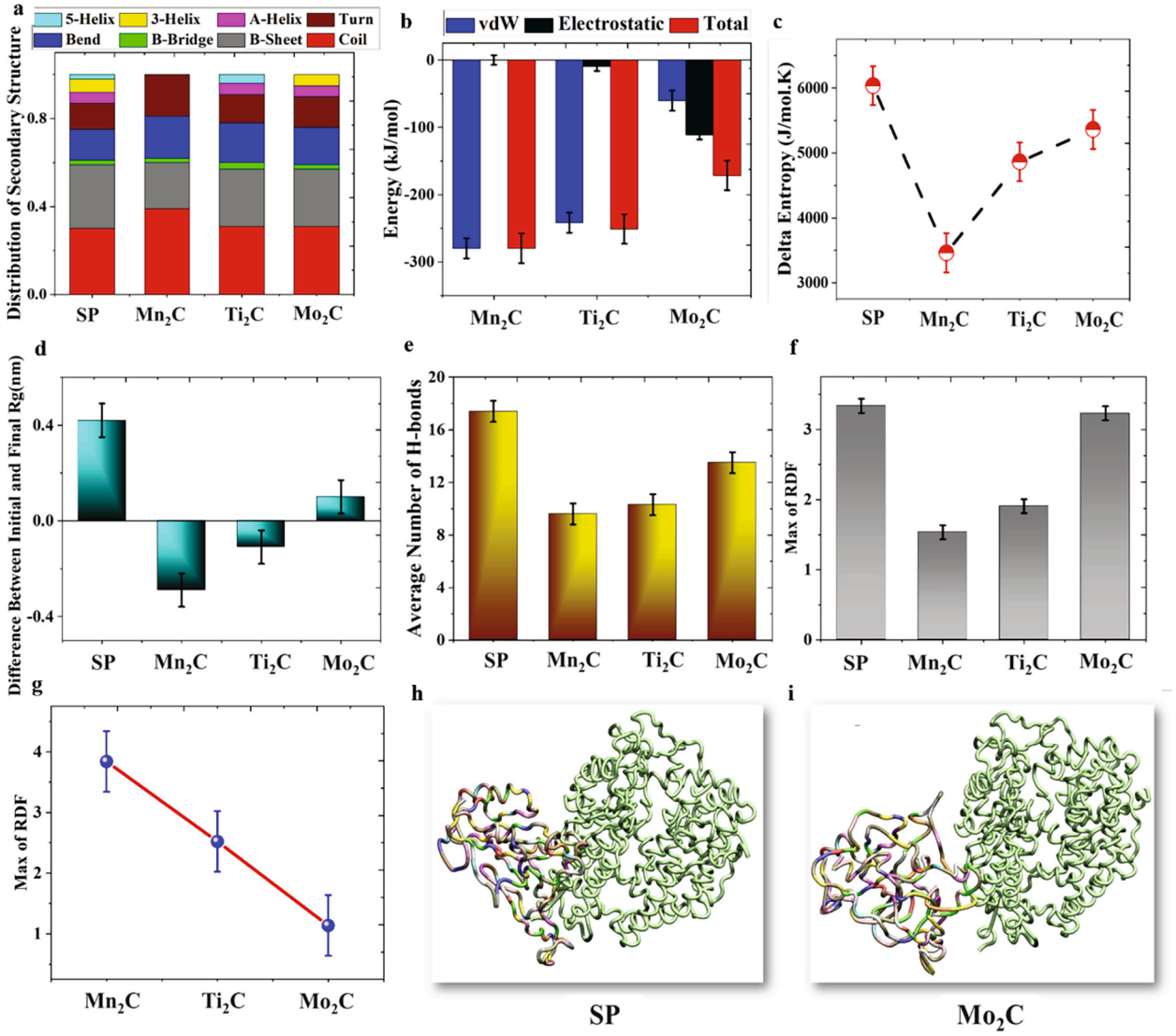

Fig. 10. (a) Composition of the secondary structures of MXene-mediated spike protein. (b) Variation in the interaction energy of spike protein and MXenes. (c) Change in entropy of the spike protein/ACE2 system. (d) Difference in the initial and final gyration radius of the MXene treated spike protein. (e) Average number of H-bonds between the deformed spike protein and ACE2. (f) Maximum RDF of the distorted spike protein in presence of ACE2. (g) Maximum RDF of the spike protein in exposure to MXene. (h) Configuration of the spike protein/ACE2 interaction. (i) Configuration of the MXene-mediated spike protein/ACE2 interaction. Reproduced with permission from Ref. [73], Copyright 2021, Taylor & Francis.

photoacoustic imaging features with superior biocompatibility. The excellent photodynamic properties of MXenes can lead to the treatment of virus-infected organs along with the fabrication of efficient touch-free sanitizers and sterilizers [81].

5.3. Biocompatibility and cytotoxicity

The biocompatibility and cytotoxicity of MXenes have been studied by many authors to foster their medical applications as nano agents for drug loading and vaccine delivery. Nasrallah et al. [82] studied the cytotoxicity of $Ti_3C_2T_x$ MXene using an in vivo zebrafish embryo model. The authors reported that no teratogenic or neurotoxic effect was observed in the embryo growth up to the MXene concentration of 100 μg mL^{-1}, which keeps the MXenes in the "practically nontoxic" group, according to the Acute Toxicity Rating Scale by the Fish and Wildlife Service (FWS). The toxicity of MXene was investigated at the early embryonic stage as well as during angiogenesis [83]. The authors experimented with the avian embryos at 3 and 5 days of incubation. They found an adverse effect on the early stage of embryogenesis as ~46% of the MXene treated embryos led to death within 1–5 days and inhibition of the angiogenesis of the chorioallantoic membrane of the embryo within an incubation period of 5 days. The authors also observed gene deregulation in the MXene treated embryos, confirming the toxic effect of MXene at higher concentrations. Han et al. [84] found that the $Ti_3C_2T_x$ MXenes have a superior drug loading capacity of up to 211.8% as well as on-demand point specific drug release by the pH-responsive and near-infrared laser triggering techniques. When injected intravenously into the body of the mouse, the MXenes reported a greater histocompatibility, efficient photoacoustic imaging, and their gradual excretion out of the body with no toxic effect, which makes them a promising biosafety material. The in vitro and in vivo studies of the soybean phospholipid (SP) modified Ta_4C_3 and polyvinylpyrrolidone (PVP) modified Nb_2C colloids etc. exhibited negligible toxicity when injected into the body of a mouse [78,85]. Dai et al. [86] studied the biosafety and biocompatibility of MXene based MnO_x/Ti_3C_2-SP composite by injecting its different doses into healthy Kunming mice. The authors observed no losses in weight, no tissue damage, or abnormal behavior in the mice even after an exposure of 30 days. The authors

concluded that the biocompatible natural amphiphilic molecules of SP enhanced the biocompatibility and dispersibility of MXenes.

For better exploration of MXenes as effective drug and vaccine delivery platform, the biocompatibility of MXenes towards the human immune cells has to be tested. Unal et al. [17] studied the response of human immune cells to the $Ti_3C_2T_x$ MXenes by exposing pure samples of human peripheral blood mononuclear cells (PBMCs) and immortalized human T lymphocytes (Jurkat cells) to $Ti_3C_2T_x$ for 24 hr. No cytotoxic effect was observed for the MXene treated Jurkat cells, PBMCs, CD4 + T cells or CD8 + T cells, monocytes as well as in classical monocytes (C. monocytes), non-classical monocytes (N. C. monocytes), and intermediate monocytes (Int. monocytes), etc. as compared to the EtOH 70% positive control (Fig. 11A-D) [17]. The authors also exposed $Ti_3C_2T_x$ + LPS to the stimulated PBMCs population and found a notable reduction of the CD25 activation markers as compared to the LPS positive and negative control [17]. A similar reduction in the TNFα levels of the PBMCs supernatant was found with the treatment of $Ti_3C_2T_x$ + LPS against the LPS positive control [17]. To study the impact of $Ti_3C_2T_x$ on human immune cells in detail, Unal and coworkers identified 17 clusters of differentiation markers (CD) on the cell surface of PBMCs (10), T and B cells (7) respectively, using the single-cell mass cytometry technology (CyTOF) and applied viSNE computational approach to construct single-cell resolution plot [17]. With the help of this method, the researchers found 9 remarkable immune cells (CD 45 +) populations i.e., CD4 + Th. cells, CD8 + Th. cells, B cells, C. monocytes, Int. monocytes, N. C. monocytes, natural killer cells (NKs), plasmacytoid and myeloid dendritic cells (pDCs and mDCs), respectively (Fig. 11E) [17]. Using the method of cisplatin staining, the ability of cisplatin to enter into necrotic

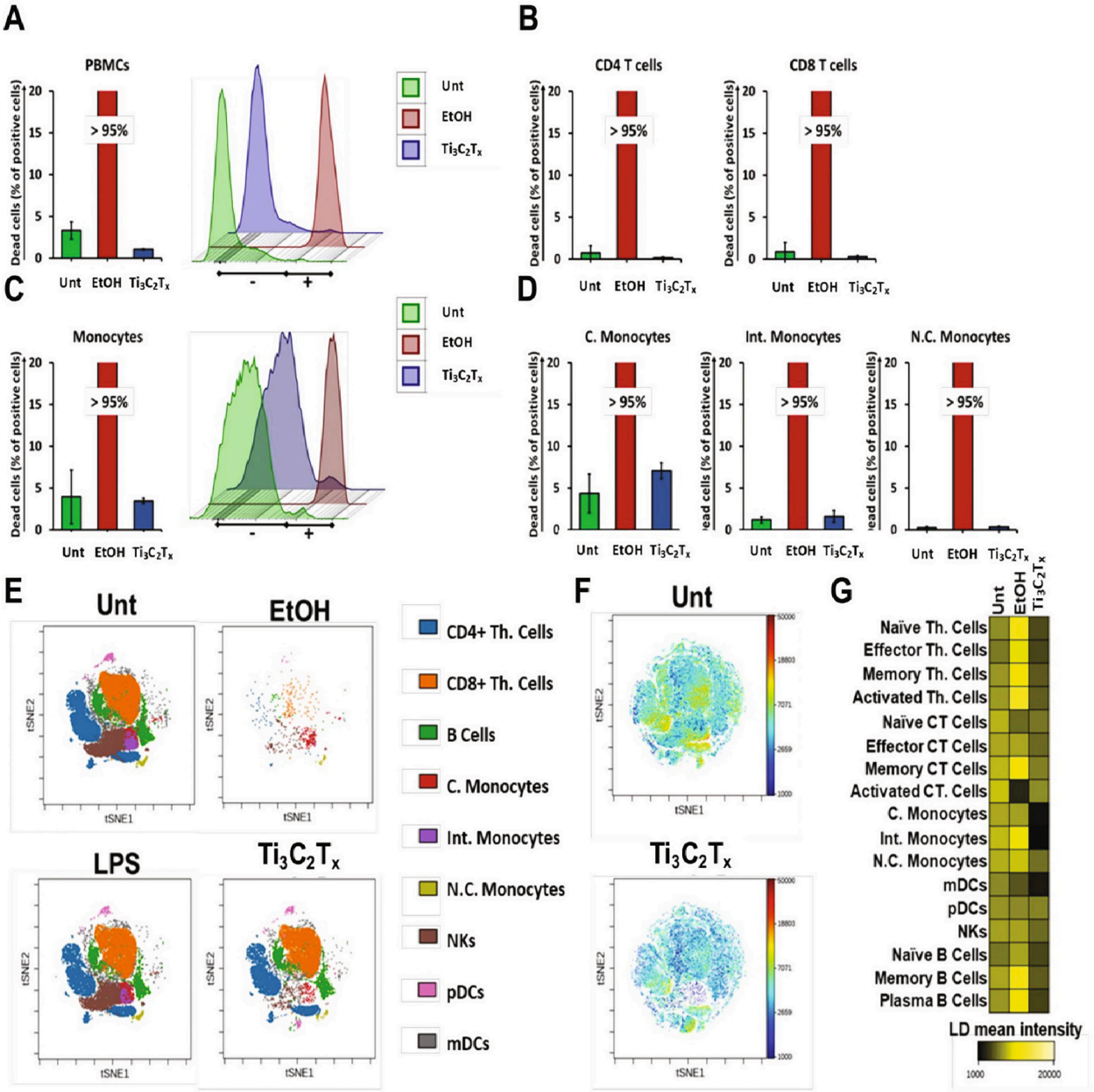

Fig. 11. Graphs illustrating the comparative study on the cytotoxicity of $Ti_3C_2T_x$ MXene and EtOH 70% positive control on the human immune cells, A) PBMCs, B) CD4 + T cells and CD8 + T cells, C) monocytes, D) C. monocytes, Int. monocytes, N. C. monocytes. E) Single-cell subpopulation cluster analysis of the $Ti_3C_2T_x$ treated nine remarkable CD markers by using viSNE technology. F) viSNE analysis of the untreated and $Ti_3C_2T_x$ treated single-cell immune sub-populations with the help of LD mean marker expressions. G) Heat map of the immune sub-populations indicating LD mean intensity. Reproduced with permission from Ref. [17], Copyright 2021, Elsevier.

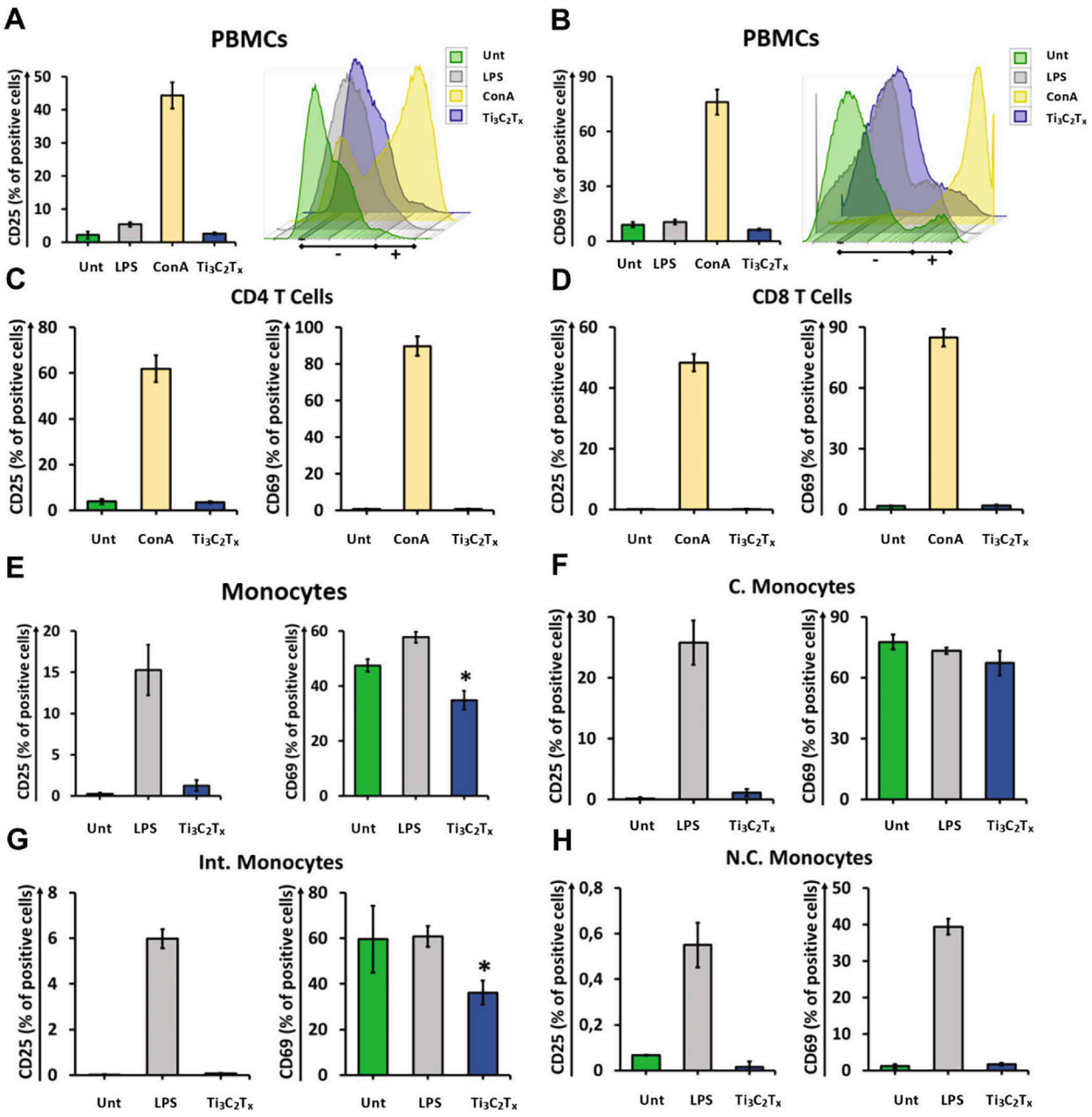

Fig. 12. Graphs indicating the viability of different immune sub-populations in the presence of $Ti_3C_2T_x$ as compared to ConA and LPS positive control. Reproduced with permission from Ref. [17], Copyright 2021, Elsevier.

and apoptotic cells, the viability of the PBMCs were studied by using the viSNE computational single-cell resolution plot and heat map indicating the LD mean marker counts (Fig. 11F, G) [17]. The study also reported no impact of the $Ti_3C_2T_x$ MXene on the functionality of the CD25 or CD69 markers for PBMCs, CD4 T cells, or CD8 T cells. Whereas a significant reduction of CD69 expression was observed for the monocytes, especially for intermediate monocytes with no change in CD25 expressions, indicating the reduction of proinflammatory activity of the intermediate monocytes (Fig. 12) [17].

The exposure of an external agent to the body results in the higher production of cytokine hormones, provoking the cytokine storm and damaging internal organs [87]. In the case of COVID-19 patients with extreme severity, there is an increased production of cytokines like TNF-α, IL-10, and IL-6, etc. which leads to the fatal condition of patients with severe damage to internal organs [87,88]. Therefore, it is crucial to remove the excess cytokines from the body in no time. To explore the impact of $Ti_3C_2T_x$ MXene on cytokine production, the researchers applied CyTOF to study the growth rate of IFN-ɣ, IL-17f, IL-17a, TNF-α, IL-6 cytokines as well as the Granzyme B and Perforin proteins that contribute to the immune response of cells [17]. The heat map reveals a feeble production rate of the cytokines indicating the anti-inflammatory properties of MXenes (Fig. 13) [17].

6. Inactivation mechanism of MXene towards SARS-CoV-2

To understand the inactivation mechanism of MXene towards the SARS-CoV-2 virus, Unal and coworkers [17] conducted the proteomic analysis of the virus-infected Vero E6 Cells in exposure to MXene. A total of 158 differentially expressed proteins were found in this study among which 68 proteins were down-regulated and 90 were up-regulated with the exposure to MXene. Gordon et al. [89] found 332 high confidence proteins after studying the interaction between the SARS-CoV-2 proteins

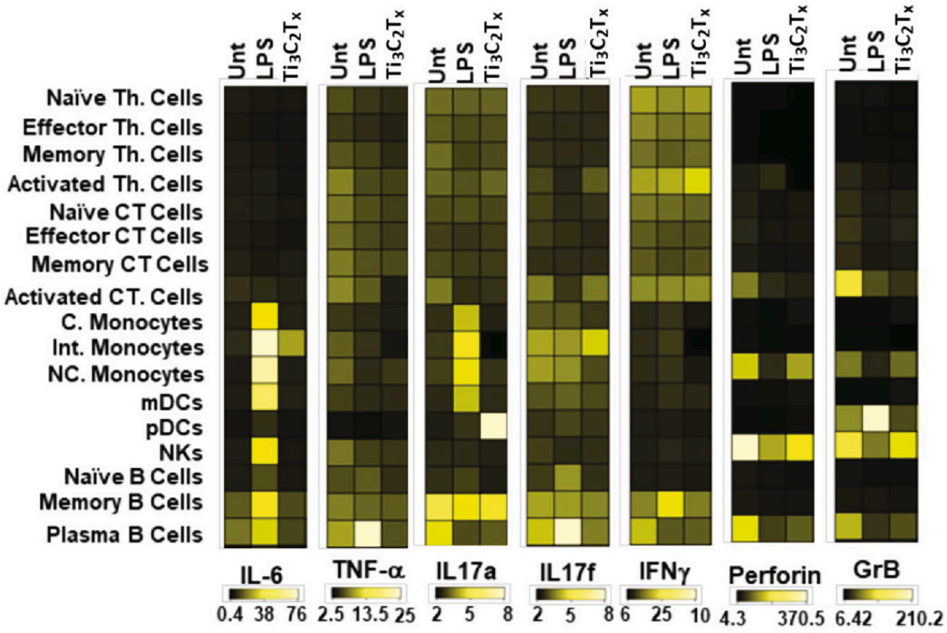

Fig. 13. Heat map indicating the lower production rate of cytokines in exposure with $Ti_3C_2T_x$ MXene as compared to untreated and LPS exposed cells. Reproduced with permission from Ref. [17], Copyright 2021, Elsevier.

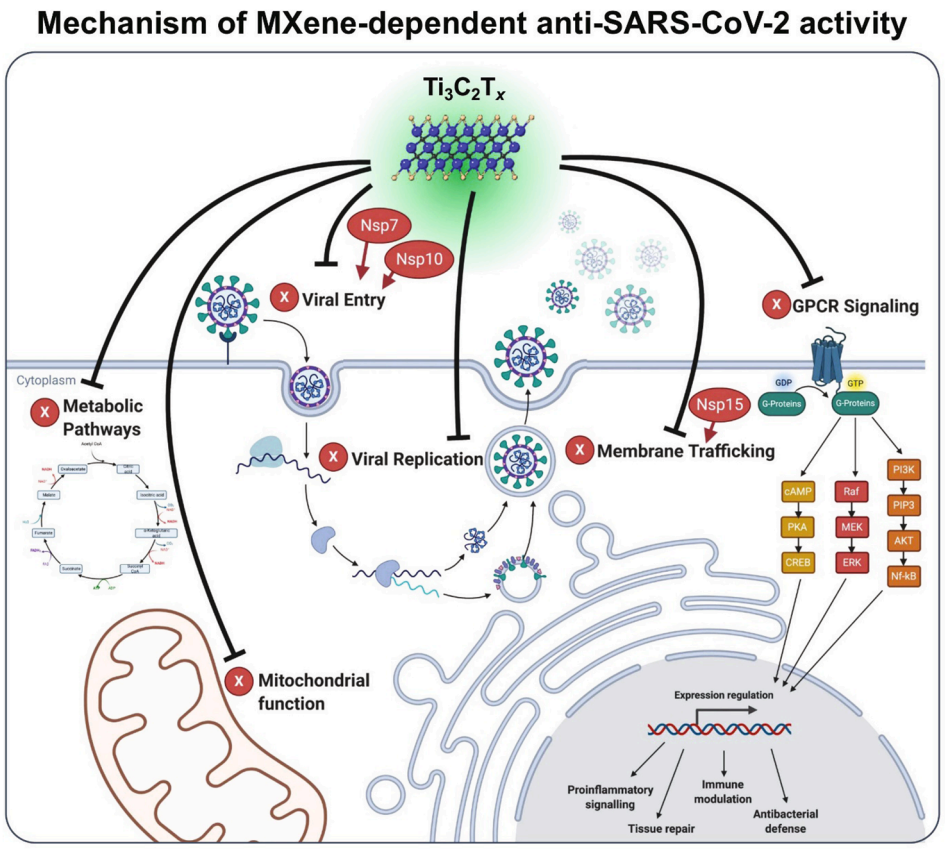

Fig. 14. Figure illustrating the SARS-CoV-2 virus inhibition mechanism by $Ti_3C_2T_x$ MXene. $Ti_3C_2T_x$ inhibits viral entry and replication through a variety of signaling pathways, including metabolic pathways, mitochondrial function, viral replication, membrane trafficking, and GPCR signaling. The host proteins NUTF2, GNG5, and GRPEL1 regulate the antiviral mechanism of $Ti_3C_2T_x$ MXene by interacting with certain SARS-CoV-2 viral proteins such as NSP15, NSP7, and NSP10. Inhibition of these signaling mechanisms in Vero E6 cells leads to the inactivation of the SARS-CoV-2 virus. Reproduced with permission from Ref. [17], Copyright 2021, Elsevier.

and human cell proteins. A comparative study with the protein dataset of $Ti_3C_2T_x$ MXenes and the dataset of Gordon et al. reported similarity of 59 interacted proteins, among them NUTF2, GNG5, and GRPEL1 are the most significant ones. These proteins interact with certain SARS-CoV-2 viral proteins such as NSP15, NSP7, and NSP10 respectively, that are involved in the different biological and metabolic pathways of the virus [90,91]. NSP15 takes part in vesicle trafficking and nuclear transport machinery. NSP7 plays a role in membrane trafficking as well as G-protein coupled receptor signaling. NSP7 and NSP10 alter the endomembrane compartments to facilitate viral entry and replication. Thus, the interaction of $Ti_3C_2T_x$ MXene with the viral signaling mechanisms in Vero E6 cells leads to inhibition of the SARS-CoV-2 virus (Fig. 14) [17].

7. Defeating COVID-19 with 2D MXene

The superior antiviral activities, greater photocatalytic/photothermal properties, and excellent biocompatibility of MXenes can be utilized in an effective way to defeat the COVID-19 pandemic. Many researchers are working worldwide to combat the pandemic and the addition of MXenes in this field can lead the research a step ahead.

7.1. Fighting with comorbidities

The COVID-19 patients having comorbidities like lung infection, kidney injury, diabetes, etc. have reported a higher mortality rate. Along with this bacterial and fungal infections and neural disorders are most likely detected and exhibited a greater impact on the health of COVID-19 patients even after recovery. Therefore, it is necessary to cure those diseases along with preventing the infection of the virus. Several reports have shown the cases of encephalitis in COVID-19 patients resulting in neural tissue degradation and other neural disorders [92]. Better treatment can be done by utilizing the high electrical conductivity of MXenes to regenerate the neural tissues and increase neuronal electrical activities (Fig. 15) [93]. Studies have shown that the porous nanofiber scaffolds enhance tissue regeneration by promoting cell adhesion, cell growth, diffusion of nutrients and vascularization, etc. [94,95]. This porosity and high surface area of the nanofiber scaffolds can be achieved by utilizing the unique layered structure of MXenes [96].

The COVID-19 infected patients have also reported a coinfection of bacteria and fungi in the respiratory tract, which needs antimicrobial therapy [97]. MXenes can be a potent material in this regard due to their antimicrobial properties. Lim et al. studied the antifungal properties of MXenes by growing the fungus *tricoderma reesei* on delaminated $Ti_3C_2T_x$ nanosheets and found no germination of hyphae and spores even after a culture of 11 days (Fig. 16) [98]. Shamsabadi et al. exposed the samples of *Bacillus subtilis* and *Escherichia coli* to the colloidal solution of MXene nanosheets and observed the release of bacterial DNA within 3hrs of cultures followed by the bacterial cell dispersion as a result of the strong interaction between the MXene nanosheets and bacterial cell membrane (Fig. 17) [99].

7.2. Drug delivery applications

The high aspect ratio and greater hydrophilicity of MXenes with lesser cytotoxicity provide a great promise for higher drug loading and point-specific drug delivery to the internal organs like lungs, specifically in the case of SARS-CoV-2 virus-infected patients [100]. Liu et al. [101] reported a superior drug loading capacity of 225.05% in the case of Ti_3C_2-cobalt nanowire heterojunction based nanocarriers. The hydrogel nanocomposites of Ti_3C_2/polyacrylamide exhibited greater drug loading of 97.5–127.7 mg g^{-1} and drug release ability of 62.1%-81.4%, respectively [16]. The superior hydrophilicity of MXenes can provide a greater solubility with the body fluids and can efficiently enhance the drug uptake by body tissues [102]. Higher drug loading and facile encapsulation methods for structured drug delivery can be achieved by the tunable surface chemistry of MXenes [7,103]. Wu et al. [104] fabricated pH/near-infrared multi-responsive microcapsules consisting of hollow hydroxyapatite, chitosan/hyaluronic acid multilayers, gold nanorods, and MXene by a layer-by-layer approach. The microcapsules were loaded with doxorubicin, which is a potential therapeutic drug against SARS-CoV-2 [105]. The fabricated microcapsules exhibited a greater drug loading capacity, distinct photothermal conversion efficiency, and biocompatibility. This property can be beneficial for remotely controlled drug delivery applications.

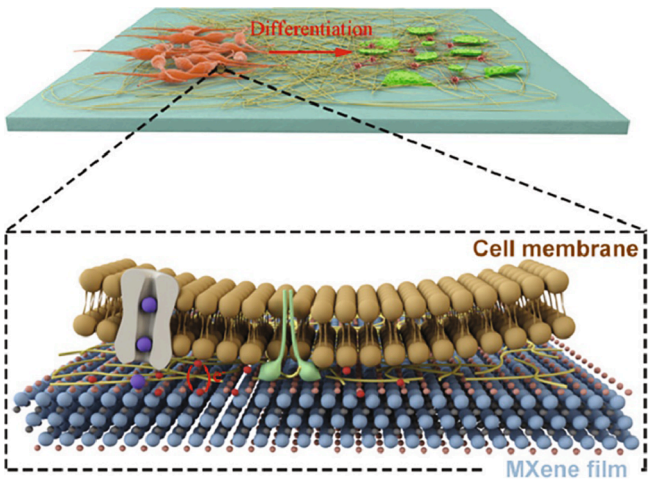

Fig. 15. Illustration of neural tissue regeneration using the high electrical conductivity of MXenes. Reproduced with permission from Ref. [93], Copyright 2020, Elsevier.

7.3. Biomedical instrumentations

The hydrophilic nature and negative surface functionalization of MXenes can be combined to fabricate different biomedical instruments like biosensors, dialyzers, sterilizers, etc. COVID-19 patients under hemodialysis are more prone to infection due to the non-removal of uremic toxins from the body [106]. Meng et al. [107] reported an adsorption efficiency of up to 94% between MXene and urea, which helps in the removal of uremic toxins from the dialysate in the case of patients under hemodialysis. The authors also observed greater urea adsorption for the $Ti_3C_2T_x$ MXene as compared to the Ti_2CT_x and $Mo_2TiC_2T_x$ MXenes and improved cell life with the exposure of MXene up to 24 h, making it a suitable material for biomedical applications [107]. The combination of paramagnetic behavior along with the high atomic number of MXenes results in incomparable attenuation of X rays, which can be useful for the computed tomography (CT) scanning of the virus-affected lungs to measure the extent of infection followed by appropriate diagnosis [108].

The excess release of cytokines in SARS-CoV-2 virus-infected patients results in CRS and lymphocytic apoptosis leading to a detrimental impact on the internal organs [87]. Studies have shown improved survival of early-stage sepsis patients by the removal of cytokines from the bloodstream [109]. The porous carbon structure of MXene can be implemented to adsorb the cytokines like IL-6, IL-10, TNF-α, etc. using extracorporeal perfusion (ECP) techniques, which are the major inflammatory factors in COVID-19 patients [96,110]. Wang et al. [23] used $Ti_3C_2T_x$ MXene nanosheet as an absorbent in the hemoperfusion therapy to remove cytokines from the blood of COVID-19 patients (Fig. 18). They found that MXene sheets have efficient removal capacities of the cytokines like IL-6, which is approximately 13.4% higher than the conventional activated carbon absorbents. Molecular-level analysis revealed that the hydrogen bonding between IL-6 and MXene nanosheets promotes absorption and the transformation of the secondary structure of IL-6 from α-helix to β-sheet results in their immobilization. The authors also observed greater blood compatibility with no side effects on the human blood composition.

MXenes show a great promise for biosensing activities because of their excellent physicochemical properties, greater active sites provided by enriched surface termination groups that can immobilize the biomolecules, admirable electrocatalytic activity, enhanced enzyme loading capacity provided by the larger specific surface area of the multi-layered structure, and superior biocompatibility [111,112]. Most of the patients affected by COVID-19 are found to be asymptomatic, which is a major reason for the faster spreading of the disease [113]. Therefore, early detection and diagnosis are the keys to prevent new infections. The MXene-based biosensors can play an effective role in the detection of biomarkers without any invasive methods [112]. Li et al. [19] fabricated an MXene-graphene FET sensor by using an ultrasensitive VSTM that combines the continuity of large-area high-quality

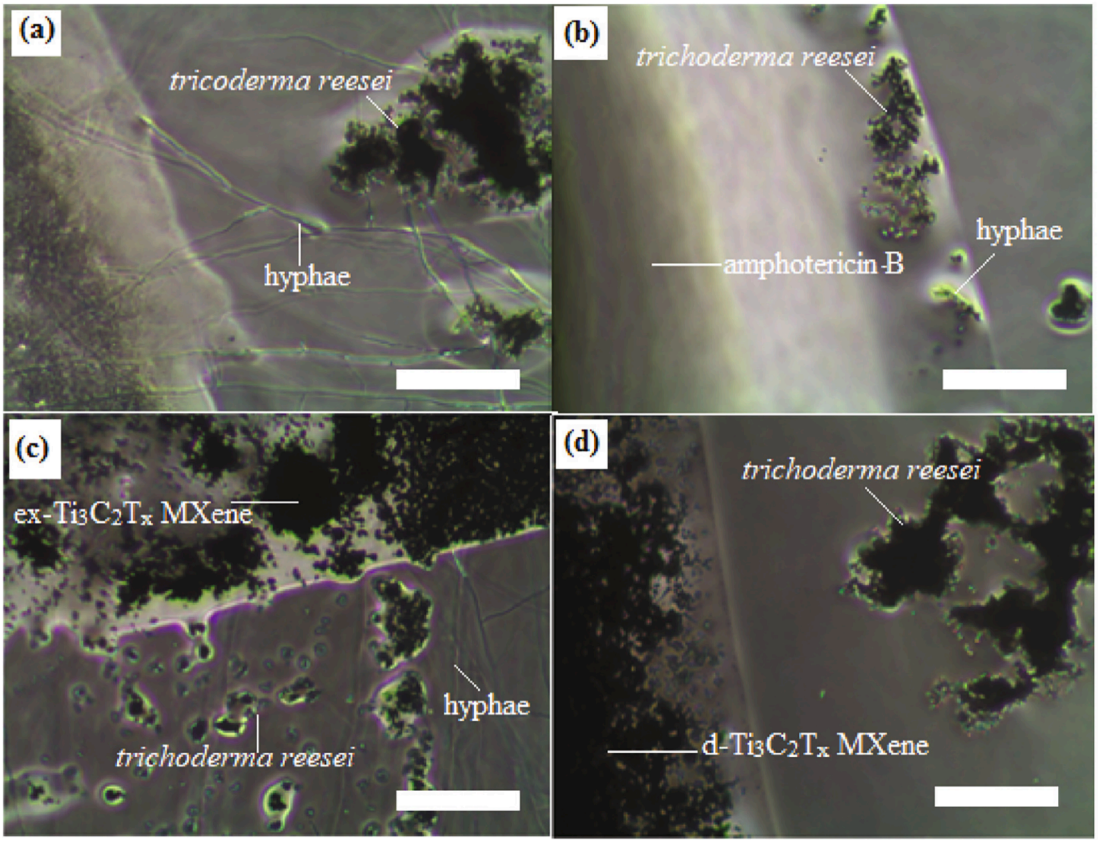

Fig. 16. The phase-contrast photomicrograph of *tricoderma reesei* fungi culture hyphae germination, revealing the antiviral activity of (a) control, (b) amphotericin, (c) ex-$Ti_3C_2T_x$ MXene nanosheets, and (d) d- $Ti_3C_2T_x$ MXene nanosheets. Reproduced with permission from Ref. [98], Copyright 2020, Elsevier.

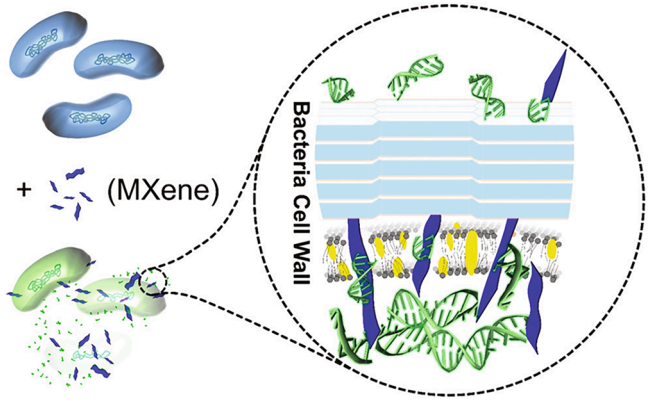

Fig. 17. Schematic of the release of bacterial DNA followed by bacterial cell dissolution by the exposure of MXene nanosheets. Reproduced with permission from Ref. [99], Copyright 2018, Americal Chemical Society.

graphene and the high chemical sensitivity of MXene. The (3-aminopropyl) triethoxysilane (APTES) functionalized VSTM were coated with SARS-CoV-2 antibodies. The binding of spike proteins to the antibodies changed the surface charge distribution of the VSTM membrane, which was observed by the electrochemical signal transduction. The fabricated device reported a low limit and wide range of detection with enhanced specificity and response time. The authors attributed this excellent result to the huge surface terminations of MXene that provides relatively greater binding sites for APTES.

Due to the lower mutation rate of nucleocapsid genomes over spike genomes, most of the national RTPCR protocols target the nucleocapsid gene for accurate detection of SARS-CoV-2 [114]. However, gene detection using RTPCR requires a tedious process of sample preparation, high-cost fluorescent probes, and a long processing time, which is not able to cope with the sudden outbreak of the pandemic. Therefore, fast and accurate detection is the need of the hour. Chen et al. [115] fabricated a single-stranded DNA (ssDNA)/ $Ti_3C_2T_x$ biosensor by the surface functionalization of ssDNA probes on $Ti_3C_2T_x$ films through noncovalent adsorption. The hybridization of the ssDNA probe with the SARS-CoV-2 nucleocapsid gene results in the detachment of double strained DNA from the $Ti_3C_2T_x$ surface, contributing to an enhanced channel conductivity (Fig. 19). The ssDNA/ $Ti_3C_2T_x$ biosensor exhibited a low limit of detection of $\sim 10^5$ copies/mL in saliva with a faster response. The authors also claimed that the self-collected saliva samples are less invasive, can reduce healthcare worker exposure, and eliminate the need for sample collecting tools like swabs.

Liu et al. [111] fabricated MXene based microfluidic biosensor chip with a combined effect of dialysis and subsequent detection of urea, uric acid, and creatinine biomarkers in the blood sample, which can help to reduce the fatality of kidney affected COVID-19 patients [106]. Studies have shown a greater rate of COVID-19 mortality in the case of patients having comorbidities, and diabetes is one of them, which reported a two-fold fatality rate [116]. The efficient and timely detection of blood glucose level by MXene-based glucose sensors can help to reduce the mortality rate to a greater extent [117]. Rakhi et al. [118] fabricated GO_x/Au/MXene/Nafion/GCE composite glucose detection biosensors having superior stability, repeatability, and reproducibility. In the glucose concentration range of 0.1 to 18 mM, the biosensor exhibited a linear amperometric response with a detection limit of 5.9 μM and greater sensitivity of 4.2 μAmM^{-1} respectively [118]. Lei et al. [119] conducted an in vitro perspiration analysis of a wearable MXene/Prussian blue-based composite biosensor and found sensitivity of up to 35.3 μAmM^{-1} cm^{-2} for glucose detection. Along with these, MXene-based biomedical instruments like pulse oximeters, respirators, sterilizers,

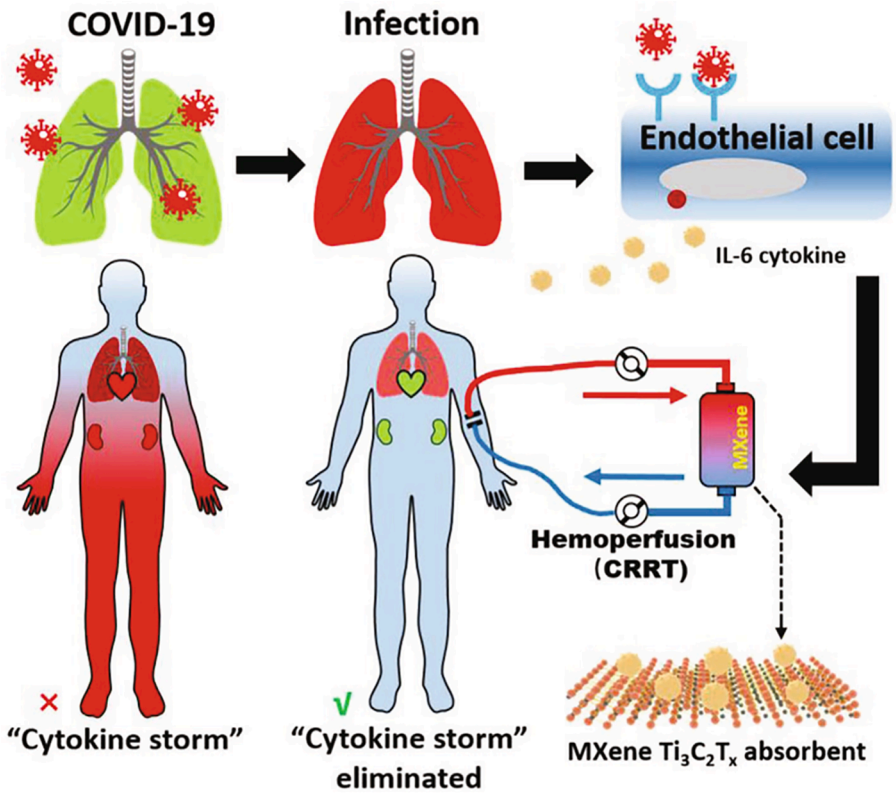

Fig. 18. Schematic illustrating the hemoperfusion therapy in COVID-19 patients using $Ti_3C_2T_x$ MXene nanosheet as an absorbent. Reproduced with permission from Ref. [23], Copyright 2021, John Wiley and Sons.

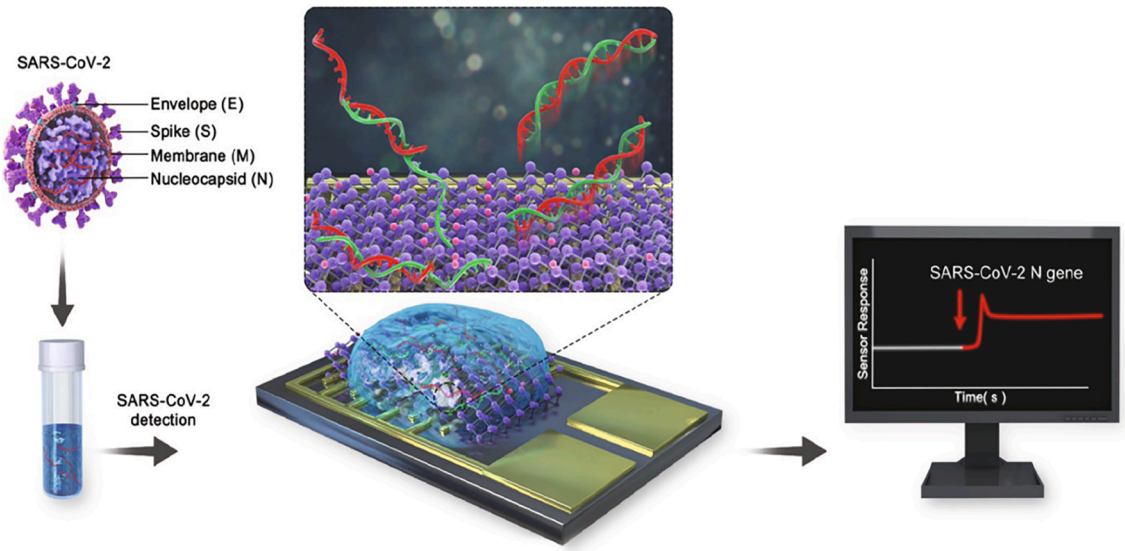

Fig. 19. Schematic illustrating the detection of SARS-CoV-2 nucleocapsid gene and variation in the sensing response of ssDNA/ $Ti_3C_2T_x$ biosensor. Adapted from Ref. [115], Copyright 2021, American Chemical Society.

ventilator components, etc. can be fabricated by using the facile 3D printing methods [120].

Researchers have reported cases of sudden cardiac death in COVID-19 patients [121]. To mitigate this high rate of mortality, regular assessment of biomarkers like Cardiac troponin I (cTnI) is greatly required for patients having myocardial injuries like acute myocardial infarction [122]. Mi et al. [123] developed a ratiometric sensing technology based on the referable EC signal of Dox *vs*. the electrochemical signal of methylene blue or electrochemiluminescent signal of doxorubicin-luminol. The greater specificity of TrO_4-aptamer for cTnI binding and the superior sensing matrix of the tetrahedral DNA anchored Au/Ti_3C_2 MXene along with the improved sensitivity provided by the in situ hybrid chain reaction amplification resulted in an effective biosensor for the accurate assay of cTnI biomarkers [123]. Peng et al. [124] synthesized Ti_3C_2 nanosheets-based fluorescence DNA biosensors, that reported a greater selectivity and sensitivity for the detection of PCR amplified HPV-18 from the clinical samples. Similar techniques can be adopted for the SARS-CoV-2 viruses by targeting the virions, virus RNAs,

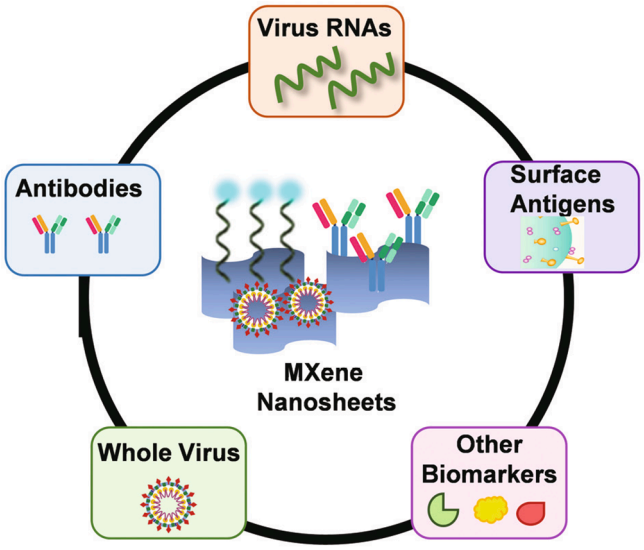

Fig. 20. Schematic illustrating the targeting of surface-functionalized MXene nanosheets to the virions, virus RNAs, virus surface antibodies/antigens, or other biomarkers, etc. of the SARS-CoV-2 virus. Adapted from Ref. [112], Copyright 2021, Royal Society of Chemistry.

virus surface antibodies/antigens, or other biomarkers, etc. by the specific surface functional group of MXene nanosheets (Fig. 20) [112].

7.4. MXene based face masks and PPE kits

Over the last few years, researchers have successfully synthesized low density, porous, and lightweight MXene foams having superior properties for biomedical applications [125]. The lightweight and porous MXene foams can fit into the requirement for pure air due to their particulate filtration properties. This particularly has a greater need in this COVID-19 pandemic situation due to the high dependence on face masks that prevents virus contaminations [126]. Although the face masks work as a virus shield, once the viruses get stuck in the outer layer of the face mask, it remains active for a longer period. Hence, proper handling and disposal of face masks have become a critical need. The major benefits of the MXene foam-based face masks is that they not only adhere to the viruses but also inactivate them by their antiviral properties [112]. Similar virus inactivation and safety methods can be achieved by the coating of MXene on PPE kits and other medical devices. These MXene based face masks, PPE kits, face shields, etc. can help to bring down the infection rate, mostly caused by COVID-19 infected asymptomatic persons [127]. Along with this, the flexibility and transparency of MXenes can also be utilized to fabricate flexible and transparent medical spectacles, face shields, etc. with antiviral properties [128].

8. Conclusion and outlook

MXenes can be a prospective material for the prevention and diagnosis of the COVID-19 disease due to their excellent antiviral activities. But some of the properties of MXenes like its hydrophilic nature are prone to environmental factors like high temperature, high moisture content, etc. which results in its surface oxidation. Thus, high temperature resistant biomedical instruments using MXene need sophisticated research. The use of antioxidants and optimization of storage conditions can further enhance the stability of MXene. Along with this, it is required to improve the antiviral properties of the MXenes and reduce their cytotoxicity, to promote its applications in biomedical fields. Reports have shown that, although MXenes are safe bioagents, in some cases they have hindered the normal functionality of internal organs like increased airway resistance in pulmonary systems by accumulating in the cytoplasm of alveolar epithelial and endothelial cells, resulting in respiratory disorder. Therefore, special care has to be taken while administrating MXene for biomedical applications. The application of MXenes and their aerosols for the development of broad-spectrum antiviral drugs especially for lung infection diagnosis has yet to be explored.

In addition to the prevention and diagnosis of the disease, the use of MXene to build a virus-free environment is the need of the future. Although MXenes were discovered a decade ago, the antiviral properties of MXenes have not been much explored yet. There is very little literature exists on its antiviral applications. With a deep understanding of the viral interaction with MXene, their properties can be further modified to enhance their antiviral behavior. The composite of MXenes with other metals and their nanoparticles (e.g. Cu, Ag, Au, etc.) having antiviral properties can improve the virus inactivation. The fabrication of MXene coated antiviral face masks, PPE kits, and biomedical instruments has been done on the laboratory scale but still, it is not commercialized due to the issues of durability, scalability, and cost-effectiveness. Therefore, low-cost and high-yield green synthesis approach has to be discovered for the scalable synthesis of MXenes and their nanocomposites. Efficient synthesis methods to increase the interlayer space and surface area of MXene can expose more active sites for viral inactivation. The adhesion of MXenes, when applied as a coating on metals and polymer surfaces is still one of the primary difficulties that have to be addressed. As in the future, many pandemics will grasp the world due to extreme environmental degradation, researchers should get ready to face those with their incredible innovations on antiviral MXene. Not only the innovations but also the transition of MXene antiviral therapy from bench to bedsides is highly required.

CRediT authorship contribution statement

Subhasree Panda: Investigation, Visualization, Writing – original draft. **Kalim Deshmukh:** Methodology, Validation, Formal analysis, Investigation, Visualization, Writing – review & editing. **Chaudhery Mustansar Hussain:** Conceptualization, Visualization, Project administration, Supervision. **S.K. Khadheer Pasha:** Visualization, Investigation, Project administration, Supervision.

Declaration of Competing Interest

The authors declare that they have no known competing financial interests or personal relationships that could have appeared to influence the work reported in this paper.

References

[1] Pandemics That Changed History: Timeline - HISTORY, (n.d.). https://www.history.com/topics/middle-ages/pandemics-timeline (accessed August 16, 2021).
[2] COVID Live Update: 241,080,676 Cases and 4,908,305 Deaths from the Coronavirus - Worldometer, (n.d.). https://www.worldometers.info/coronavirus/ (accessed October 17, 2021).
[3] WHO | World Health Organization, (n.d.). https://www.who.int/ (accessed October 9, 2021).
[4] Q. Li, X. Guan, P. Wu, X. Wang, L. Zhou, Y. Tong, R. Ren, K.S.M. Leung, E.H. Y. Lau, J.Y. Wong, X. Xing, N. Xiang, Y. Wu, C. Li, Q.i. Chen, D. Li, T. Liu, J. Zhao, M. Liu, W. Tu, C. Chen, L. Jin, R. Yang, Q.i. Wang, S. Zhou, R. Wang, H. Liu, Y. Luo, Y. Liu, G.e. Shao, H. Li, Z. Tao, Y. Yang, Z. Deng, B. Liu, Z. Ma, Y. Zhang, G. Shi, T.T.Y. Lam, J.T. Wu, G.F. Gao, B.J. Cowling, B.o. Yang, G.M. Leung, Z. Feng, Early transmission dynamics in Wuhan, China, of novel coronavirus–infected pneumonia, N. Engl. J. Med. 382 (13) (2020) 1199–1207.
[5] J. Valizadeh, A. Hafezalkotob, S.M.S. Alizadeh, P. Mozafari, Hazardous infectious waste collection and government aid distribution during COVID-19: a robust mathematical leader-follower model approach, Sustain. Cities Soc. 69 (2021), 102814.
[6] T. Yadavalli, D. Shukla, Role of metal and metal oxide nanoparticles as diagnostic and therapeutic tools for highly prevalent viral infections, Nanomedicine Nanotechnology, Biol. Med. 13 (2017) 219–230.
[7] C. Weiss, M. Carriere, L. Fusco, I. Capua, J.A. Regla-Nava, M. Pasquali, J.A. Scott, F. Vitale, M.A. Unal, C. Mattevi, D. Bedognetti, A. Merkoçi, E. Tasciotti,

A. Yilmazer, Y. Gogotsi, F. Stellacci, L.G. Delogu, Toward nanotechnology-enabled approaches against the COVID-19 pandemic, ACS Nano. 14 (6) (2020) 6383–6406.
[8] F. Amanat, F. Krammer, SARS-CoV-2 vaccines: status report, Immunity. 52 (4) (2020) 583–589.
[9] M. Yu, J. Wu, J. Shi, O.C. Farokhzad, Nanotechnology for protein delivery: overview and perspectives, J. Control. Release. 240 (2016) 24–37.
[10] A.M. Jastrzębska, A.S. Vasilchenko, Smart and Sustainable Nanotechnological Solutions in a Battle against COVID-19 and Beyond: a critical review, ACS Sustain. Chem. Eng. 9 (2) (2021) 601–622.
[11] Y. Huang, C. Yang, X. Xu, W. Xu, S. Liu, Structural and functional properties of SARS-CoV-2 spike protein: potential antivirus drug development for COVID-19, Acta Pharmacol. Sin. 41 (2020) 1141–1149.
[12] Q.-S. Rao, S.-Y. Liao, X.-W. Huang, Y.-Z. Li, Y.-D. Liu, Y.-G. Min, Assembly of MXene/PP separator and its enhancement for Ni-Rich LiNi0. 8Co0. 1Mn0. 1O2 electrochemical performance, Polymers (Basel). 12 (2020) 2192.
[13] Z. You, Y. Liao, X. Li, J. Fan, Q. Xiang, State of the art recent progress in MXene-based photocatalysts: a comprehensive review, Nanoscale 13 (21) (2021) 9463–9504.
[14] Z. Huang, X. Cui, S. Li, J. Wei, P. Li, Y. Wang, C.-S. Lee, Two-dimensional MXene-based materials for photothermal therapy, Nanophotonics 9 (2020) 2233–2249.
[15] K. Deshmukh, T. Kovářík, S.K. Khadheer Pasha, State of the art recent progress in two dimensional MXenes based gas sensors and biosensors: a comprehensive review, Coord. Chem. Rev. 424 (2020) 213514.
[16] P. Zhang, X.-J. Yang, P. Li, Y. Zhao, Q.J. Niu, Fabrication of novel MXene (Ti 3 C 2)/polyacrylamide nanocomposite hydrogels with enhanced mechanical and drug release properties, Soft Matter. 16 (1) (2020) 162–169.
[17] M.A. Unal, F. Bayrakdar, L. Fusco, O. Besbinar, C.E. Shuck, S. Yalcin, M.T. Erken, A. Ozkul, C. Gurcan, O. Panatli, 2D MXenes with antiviral and immunomodulatory properties: a pilot study against SARS-CoV-2, Nano Today. 38 (2021), 101136.
[18] G. Seo, G. Lee, M.J. Kim, S.-H. Baek, M. Choi, K.B. Ku, C.-S. Lee, S. Jun, D. Park, H.G. Kim, S.-J. Kim, J.-O. Lee, B.T. Kim, E.C. Park, S.I. Kim, Rapid detection of COVID-19 causative virus (SARS-CoV-2) in human nasopharyngeal swab specimens using field-effect transistor-based biosensor, ACS Nano. 14 (4) (2020) 5135–5142.
[19] Y. Li, Z. Peng, N.J. Holl, M.R. Hassan, J.M. Pappas, C. Wei, O.H. Izadi, Y. Wang, X. Dong, C. Wang, Y.-W. Huang, D.H. Kim, C. Wu, MXene–graphene field-effect transistor sensing of influenza virus and SARS-CoV-2, ACS Omega. 6 (10) (2021) 6643–6653.
[20] C. Ménard-Moyon, A. Bianco, K. Kalantar-Zadeh, Two-dimensional material-based biosensors for virus detection, ACS Sens. 5 (12) (2020) 3739–3769.
[21] J. Liu, X. Chen, Q. Wang, M. Xiao, D. Zhong, W. Sun, G. Zhang, Z. Zhang, Ultrasensitive monolayer MoS2 field-effect transistor based DNA sensors for screening of down syndrome, Nano Lett. 19 (3) (2019) 1437–1444.
[22] S.J. Kim, H.-J. Koh, C.E. Ren, O. Kwon, K. Maleski, S.-Y. Cho, B. Anasori, C.-K. Kim, Y.-K. Choi, J. Kim, Y. Gogotsi, H.-T. Jung, Metallic Ti3C2T x MXene gas sensors with ultrahigh signal-to-noise ratio, ACS Nano. 12 (2) (2018) 986–993.
[23] T. Wang, X. Sun, X. Guo, J. Zhang, J. Yang, S. Tao, J. Guan, L. Zhou, J. Han, C. Wang, Ultraefficiently calming cytokine storm using Ti3C2Tx MXene, Small Methods 5 (2021) 2001108.
[24] B. Anasori, Û.G. Gogotsi, 2D metal carbides and nitrides (MXenes), Springer, (2019) 3-12.
[25] G. Deysher, C.E. Shuck, K. Hantanasirisakul, N.C. Frey, A.C. Foucher, K. Maleski, A. Sarycheva, V.B. Shenoy, E.A. Stach, B. Anasori, Y. Gogotsi, Synthesis of Mo4VAlC4 MAX phase and two-dimensional Mo4VC4 MXene with five atomic layers of transition metals, ACS Nano. 14 (1) (2020) 204–217.
[26] S. Panda, K. Deshmukh, S.K.K. Pasha, J. Theerthagiri, S. Manickam, M.Y. Choi, MXene based emerging materials for supercapacitor applications: Recent advances, challenges, and future perspectives, Coord. Chem. Rev. 462 (2022), 214518.
[27] W. Hong, B.C. Wyatt, S.K. Nemani, B. Anasori, Double transition-metal MXenes: Atomistic design of two-dimensional carbides and nitrides, MRS Bull. 45 (2020) 850–861.
[28] M. Naguib, M.W. Barsoum, Y. Gogotsi, Ten years of progress in the synthesis and development of MXenes, Adv. Mater. 33 (2021) 2103393.
[29] M. Naguib, O. Mashtalir, J. Carle, V. Presser, J. Lu, L. Hultman, Y. Gogotsi, M. W. Barsoum, Two-dimensional transition metal carbides, ACS Nano 6 (2) (2012) 1322–1331.
[30] S. Venkateshalu, A.N. Grace, MXenes—A new class of 2D layered materials: synthesis, properties, applications as supercapacitor electrode and beyond, Appl. Mater. Today. 18 (2020), 100509.
[31] R.M. Ronchi, J.T. Arantes, S.F. Santos, Synthesis, structure, properties and applications of MXenes: current status and perspectives, Ceram. Int. 45 (2019) 18167–18188.
[32] L.i. Ding, Y. Wei, Y. Wang, H. Chen, J. Caro, H. Wang, A two-dimensional lamellar membrane: MXene nanosheet stacks, Angew. Chemie Int. Ed. 56 (7) (2017) 1825–1829.
[33] Y. Sun, Y. Li, Potential environmental applications of MXenes: a critical review, Chemosphere 271 (2021), 129578.
[34] A. Iqbal, P. Sambyal, C.M. Koo, 2D MXenes for electromagnetic shielding: a review, Adv. Funct. Mater. 30 (47) (2020) 2000883.
[35] X. Zhan, C. Si, J. Zhou, Z. Sun, MXene and MXene-based composites: synthesis, properties and environment-related applications, Nanoscale Horizons. 5 (2020) 235–258.
[36] O. Mashtalir, M. Naguib, V.N. Mochalin, Y. Dall'Agnese, M. Heon, M.W. Barsoum, Y. Gogotsi, Intercalation and delamination of layered carbides and carbonitrides, Nat. Commun. 4 (1) (2013).
[37] S.H. Overbury, A.I. Kolesnikov, G.M. Brown, Z. Zhang, G.S. Nair, R.L. Sacci, R. Lotfi, A.C.T. Van Duin, M. Naguib, Complexity of intercalation in MXenes: destabilization of urea by two-dimensional titanium carbide, J. Am. Chem. Soc. 140 (2018) 10305–10314.
[38] O. Mashtalir, M.R. Lukatskaya, M.-Q. Zhao, M.W. Barsoum, Y. Gogotsi, Amine-assisted delamination of Nb2C MXene for Li-ion energy storage devices, Adv. Mater. 27 (23) (2015) 3501–3506.
[39] O. Mashtalir, M.R. Lukatskaya, A.I. Kolesnikov, E. Raymundo-Piñero, M. Naguib, M.W. Barsoum, Y. Gogotsi, The effect of hydrazine intercalation on the structure and capacitance of 2D titanium carbide (MXene), Nanoscale 8 (17) (2016) 9128–9133.
[40] M. Naguib, R.R. Unocic, B.L. Armstrong, J. Nanda, Large-scale delamination of multi-layers transition metal carbides and carbonitrides "MXenes", Dalt. Trans. 44 (20) (2015) 9353–9358.
[41] M. Alhabeb, K. Maleski, B. Anasori, P. Lelyukh, L. Clark, S. Sin, Y. Gogotsi, Guidelines for synthesis and processing of two-dimensional titanium carbide (Ti3C2T x MXene), Chem. Mater. 29 (18) (2017) 7633–7644.
[42] H. Wang, J. Zhang, Y. Wu, H. Huang, G. Li, X. Zhang, Z. Wang, Surface modified MXene Ti3C2 multilayers by aryl diazonium salts leading to large-scale delamination, Appl. Surf. Sci. 384 (2016) 287–293.
[43] M.R. Lukatskaya, O. Mashtalir, C.E. Ren, Y. Dall'Agnese, P. Rozier, P.L. Taberna, M. Naguib, P. Simon, M.W. Barsoum, Y. Gogotsi, Cation intercalation and high volumetric capacitance of two-dimensional titanium carbide, Science 341 (2013) 1502–1505.
[44] M. Naguib, M. Kurtoglu, V. Presser, J. Lu, J. Niu, M. Heon, L. Hultman, Y. Gogotsi, M.W. Barsoum, Two-dimensional nanocrystals produced by exfoliation of Ti3AlC2, Adv. Mater. 23 (37) (2011) 4248–4253.
[45] M. Khazaei, M. Arai, T. Sasaki, A. Ranjbar, Y. Liang, S. Yunoki, OH-terminated two-dimensional transition metal carbides and nitrides as ultralow work function materials, Phys. Rev. B. 92 (2015) 75411.
[46] M. Ghidiu, M.R. Lukatskaya, M.-Q. Zhao, Y. Gogotsi, M.W. Barsoum, Conductive two-dimensional titanium carbide 'clay'with high volumetric capacitance, Nature 516 (7529) (2014) 78–81.
[47] J. Halim, S. Kota, M.R. Lukatskaya, M. Naguib, M.-Q. Zhao, E.J. Moon, J. Pitock, J. Nanda, S.J. May, Y. Gogotsi, M.W. Barsoum, Synthesis and characterization of 2D molybdenum carbide (MXene), Adv. Funct. Mater. 26 (18) (2016) 3118–3127.
[48] F. Liu, J. Zhou, S. Wang, B. Wang, C. Shen, L. Wang, Q. Hu, Q. Huang, A. Zhou, Preparation of high-purity V2C MXene and electrochemical properties as Li-ion batteries, J. Electrochem. Soc. 164 (4) (2017) A709–A713.
[49] F. Du, H. Tang, L. Pan, T. Zhang, H. Lu, J. Xiong, J. Yang, C.J. Zhang, Environmental friendly scalable production of colloidal 2D titanium carbonitride MXene with minimized nanosheets restacking for excellent cycle life lithium-ion batteries, Electrochim. Acta 235 (2017) 690–699.
[50] T. Zhang, L. Pan, H. Tang, F. Du, Y. Guo, T. Qiu, J. Yang, Synthesis of two-dimensional Ti3C2Tx MXene using HCl+ LiF etchant: enhanced exfoliation and delamination, J. Alloys Compd. 695 (2017) 818–826.
[51] P. Zhang, L. Wang, K. Du, S. Wang, Z. Huang, L. Yuan, Z. Li, H. Wang, L. Zheng, Z. Chai, Effective removal of U (VI) and Eu (III) by carboxyl functionalized MXene nanosheets, J. Hazard. Mater. 396 (2020), 122731.
[52] J. Halim, M.R. Lukatskaya, K.M. Cook, J. Lu, C.R. Smith, L.-Å. Näslund, S.J. May, L. Hultman, Y. Gogotsi, P. Eklund, M.W. Barsoum, Transparent conductive two-dimensional titanium carbide epitaxial thin films, Chem. Mater. 26 (7) (2014) 2374–2381.
[53] M. Naguib, T. Saito, S. Lai, M.S. Rager, T. Aytug, M. Parans Paranthaman, M.-Q. Zhao, Y. Gogotsi, Ti 3 C 2 T x (MXene)–polyacrylamide nanocomposite films, RSC Adv. 6 (76) (2016) 72069–72073.
[54] C. Xu, L. Wang, Z. Liu, L. Chen, J. Guo, N. Kang, X.-L. Ma, H.-M. Cheng, W. Ren, Large-area high-quality 2D ultrathin Mo 2 C superconducting crystals, Nat. Mater. 14 (11) (2015) 1135–1141.
[55] J. Jia, T. Xiong, L. Zhao, F. Wang, H. Liu, R. Hu, J. Zhou, W. Zhou, S. Chen, Ultrathin N-doped Mo2C nanosheets with exposed active sites as efficient electrocatalyst for hydrogen evolution reactions, ACS Nano 11 (12) (2017) 12509–12518.
[56] F. Zhang, Z. Zhang, H. Wang, C.H. Chan, N.Y. Chan, X.X. Chen, J.-Y. Dai, Plasma-enhanced pulsed-laser deposition of single-crystalline M o 2 C ultrathin superconducting films, Phys. Rev. Mater. 1 (2017) 34002.
[57] Y. Wei, P. Zhang, R.A. Soomro, Q. Zhu, B. Xu, Advances in the synthesis of 2D Mxenes, Adv. Mater. 33 (2021) 2103148.
[58] M.A. Hasan, A. Carmel Mary Esther, A. Dey, A.K. Mukhopadhyay, A review on coronavirus survivability on material's surfaces: present research scenarios, technologies and future directions, Surf. Eng. 36 (2020) 1226–1239.
[59] A.R. Fehr, S. Perlman, Coronaviruses: an overview of their replication and pathogenesis, Coronaviruses 1282 (2015) 1–23.
[60] J.S.M. Peiris, K.Y. Yuen, A.D.M.E. Osterhaus, K. Stöhr, The severe acute respiratory syndrome, N. Engl. J. Med. 349 (25) (2003) 2431–2441.
[61] R.L. Graham, E.F. Donaldson, R.S. Baric, A decade after SARS: strategies for controlling emerging coronaviruses, Nat. Rev. Microbiol. 11 (2013) 836–848.
[62] Novel Coronavirus (2019-nCoV) situation reports, (n.d.). https://www.who.int/timorleste/emergencies/novel-coronavirus-2019/novel-coronavirus-(2019-ncov)-situation-reports (accessed October 17, 2021).
[63] Y.A. Agabi, I. Shittu, K.I. Amagon, J.G. Damen, R.J. Kutshik, U. Ajima, B.B. Bukar, K.D. Falang, I.Y. Longdet, S.S. Gomerep, S.D. Davou, J.A. Kolawole, N. N. Wannang, Consequences of mutations in severe acute respiratory syndrome

Coronavirus 2 (Sars-Cov-2) Genome in comparison to other pathogenic coronaviruses, Eur. J. Biol. Biotechnol. 2 (2) (2021) 119–123.
[64] P. Zhou, X.-L. Yang, X.-G. Wang, B. Hu, L. Zhang, W. Zhang, H.-R. Si, Y. Zhu, B. Li, C.-L. Huang, H.-D. Chen, J. Chen, Y. Luo, H. Guo, R.-D. Jiang, M.-Q. Liu, Y. Chen, X.-R. Shen, X.i. Wang, X.-S. Zheng, K. Zhao, Q.-J. Chen, F. Deng, L.-L. Liu, B. Yan, F.-X. Zhan, Y.-Y. Wang, G.-F. Xiao, Z.-L. Shi, A pneumonia outbreak associated with a new coronavirus of probable bat origin, Nature 579 (7798) (2020) 270–273.
[65] GISAID - Initiative, (n.d.). https://www.gisaid.org/ (accessed October 15, 2021).
[66] S. Isabel, L. Graña-Miraglia, J.M. Gutierrez, C. Bundalovic-Torma, H.E. Groves, M. R. Isabel, AliReza Eshaghi, S.N. Patel, J.B. Gubbay, T. Poutanen, D.S. Guttman, S. M. Poutanen, Evolutionary and structural analyses of SARS-CoV-2 D614G spike protein mutation now documented worldwide, Sci. Rep. 10 (1) (2020).
[67] I.O. Omotuyi, O. Nash, O.B. Ajiboye, C.G. Iwegbulam, E.B. Oyinloye, O. A. Oyedeji, Z.A. Kashim, K. Okaiyeto, Atomistic simulation reveals structural mechanisms underlying D614G spike glycoprotein-enhanced fitness in SARS-COV-2, J. Comput. Chem. 41 (2020) 2158–2161.
[68] B. Korber, W.M. Fischer, S. Gnanakaran, H. Yoon, J. Theiler, W. Abfalterer, N. Hengartner, E.E. Giorgi, T. Bhattacharya, B. Foley, Tracking changes in SARS-CoV-2 spike: evidence that D614G increases infectivity of the COVID-19 virus, Cell. 182 (2020) 812–827.
[69] Q. Wang, Y. Zhang, L. Wu, S. Niu, C. Song, Z. Zhang, G. Lu, C. Qiao, Y.u. Hu, K.-Y. Yuen, Q. Wang, H. Zhou, J. Yan, J. Qi, Structural and functional basis of SARS-CoV-2 entry by using human ACE2, Cell 181 (4) (2020) 894–904.e9.
[70] T. Hirano, M. Murakami, COVID-19: a new virus, but a familiar receptor and cytokine release syndrome, Immunity 52 (2020) 731–733.
[71] N. Kipshidze, N. Yeo, N. Kipshidze, Photodynamic therapy for COVID-19, Nat. Photonics 14 (11) (2020) 651–652.
[72] C. Chen, M. Boota, P. Urbankowski, B. Anasori, L. Miao, J. Jiang, Y. Gogotsi, Effect of glycine functionalization of 2D titanium carbide (MXene) on charge storage, J. Mater. Chem. A. 6 (11) (2018) 4617–4622.
[73] E. Ghasemy, A. Miri Jahromi, M. Khedri, P. Zandi, R. Maleki, L. Tayebi, In-silico study on viability of MXenes in suppressing the coronavirus infection and distribution, J. Biomol. Struct. Dyn. (2021) 1–7.
[74] A. Champagne, J.-C. Charlier, Physical properties of 2D MXenes: from a theoretical perspective, J. Phys. Mater. 3 (2020) 32006.
[75] D. Gupta, Effect of ambient temperature on COVID-19 infection rate, Available SSRN 3558470 (2020).
[76] H.F. Rabenau, J. Cinatl, B. Morgenstern, G. Bauer, W. Preiser, H.W. Doerr, Stability and inactivation of SARS coronavirus, Med. Microbiol. Immunol. 194 (1-2) (2005) 1–6.
[77] R. Li, L. Zhang, L. Shi, P. Wang, MXene Ti3C2: an effective 2D light-to-heat conversion material, ACS Nano. 11 (2017) 3752–3759.
[78] H. Lin, Y. Wang, S. Gao, Y. Chen, J. Shi, Theranostic 2D tantalum carbide (MXene), Adv. Mater. 30 (2018) 1703284.
[79] K. Khorsandi, S. Fekrazad, F. Vahdatinia, A. Farmany, R. Fekrazad, Nano antiviral photodynamic therapy: a probable biophysicochemical management modality in SARS-CoV-2, Expert Opin. Drug Deliv. 18 (2) (2021) 265–272.
[80] Q. Zhang, W. Huang, C. Yang, F. Wang, C. Song, Y. Gao, Y. Qiu, M. Yan, B. Yang, C. Guo, The theranostic nanoagent Mo 2 C for multi-modal imaging-guided cancer synergistic phototherapy, Biomater. Sci. 7 (7) (2019) 2729–2739.
[81] J. Huang, Z. Li, Y. Mao, Z. Li, Progress and biomedical applications of MXenes, Nano Sel. 2 (8) (2021) 1480–1508.
[82] G.K. Nasrallah, M. Al-Asmakh, K. Rasool, K.A. Mahmoud, Ecotoxicological assessment of Ti 3 C 2 T x (MXene) using a zebrafish embryo model, Environ. Sci. Nano. 5 (4) (2018) 1002–1011.
[83] H. Alhussain, R. Augustine, E.A. Hussein, I. Gupta, A. Hasan, A.-E. Al Moustafa, A. Elzatahry, MXene nanosheets may induce toxic effect on the early stage of embryogenesis, J. Biomed. Nanotechnol. 16 (3) (2020) 364–372.
[84] X. Han, J. Huang, H. Lin, Z. Wang, P. Li, Y. Chen, 2D ultrathin MXene-based drug-delivery nanoplatform for synergistic photothermal ablation and chemotherapy of cancer, Adv. Healthc. Mater. 7 (2018) 1701394.
[85] H. Lin, S. Gao, C. Dai, Y.u. Chen, J. Shi, A two-dimensional biodegradable niobium carbide (MXene) for photothermal tumor eradication in NIR-I and NIR-II biowindows, J. Am. Chem. Soc. 139 (45) (2017) 16235–16247.
[86] C. Dai, H. Lin, G. Xu, Z. Liu, R. Wu, Y.u. Chen, Biocompatible 2D titanium carbide (MXenes) composite nanosheets for pH-responsive MRI-guided tumor hyperthermia, Chem. Mater. 29 (20) (2017) 8637–8652.
[87] P. Mehta, D.F. McAuley, M. Brown, E. Sanchez, R.S. Tattersall, J.J. Manson, COVID-19: consider cytokine storm syndromes and immunosuppression, Lancet 395 (2020) 1033–1034.
[88] G. Chen, D.i. Wu, W. Guo, Y. Cao, D. Huang, H. Wang, T. Wang, X. Zhang, H. Chen, H. Yu, X. Zhang, M. Zhang, S. Wu, J. Song, T. Chen, M. Han, S. Li, X. Luo, J. Zhao, Q. Ning, Clinical and immunological features of severe and moderate coronavirus disease 2019, J. Clin. Invest. 130 (5) (2020) 2620–2629.
[89] D.E. Gordon, G.M. Jang, M. Bouhaddou, J. Xu, K. Obernier, K.M. White, M. J. O'Meara, V.V. Rezelj, J.Z. Guo, D.L. Swaney, T.A. Tummino, R. Hüttenhain, R. M. Kaake, A.L. Richards, B. Tutuncuoglu, H. Foussard, J. Batra, K. Haas, M. Modak, M. Kim, P. Haas, B.J. Polacco, H. Braberg, J.M. Fabius, M. Eckhardt, M. Soucheray, M.J. Bennett, M. Cakir, M.J. McGregor, Q. Li, B. Meyer, F. Roesch, T. Vallet, A. Mac Kain, L. Miorin, E. Moreno, Z.Z.C. Naing, Y. Zhou, S. Peng, Y. Shi, Z. Zhang, W. Shen, I.T. Kirby, J.E. Melnyk, J.S. Chorba, K. Lou, S.A. Dai, I. Barrio-Hernandez, D. Memon, C. Hernandez-Armenta, J. Lyu, C.J.P. Mathy, T. Perica, K.B. Pilla, S.J. Ganesan, D.J. Saltzberg, R. Rakesh, X.i. Liu, S. B. Rosenthal, L. Calviello, S. Venkataramanan, J. Liboy-Lugo, Y. Lin, X.-P. Huang, YongFeng Liu, S.A. Wankowicz, M. Bohn, M. Safari, F.S. Ugur, C. Koh, N.S. Savar, Q.D. Tran, D. Shengjuler, S.J. Fletcher, M.C. O'Neal, Y. Cai, J.C.J. Chang, D. J. Broadhurst, S. Klippsten, P.P. Sharp, N.A. Wenzell, D. Kuzuoglu-Ozturk, H.-Y. Wang, R. Trenker, J.M. Young, D.A. Cavero, J. Hiatt, T.L. Roth, U. Rathore, A. Subramanian, J. Noack, M. Hubert, R.M. Stroud, A.D. Frankel, O.S. Rosenberg, K.A. Verba, D.A. Agard, M. Ott, M. Emerman, N. Jura, M. von Zastrow, E. Verdin, A. Ashworth, O. Schwartz, C. d'Enfert, S. Mukherjee, M. Jacobson, H.S. Malik, D. G. Fujimori, T. Ideker, C.S. Craik, S.N. Floor, J.S. Fraser, J.D. Gross, A. Sali, B. L. Roth, D. Ruggero, J. Taunton, T. Kortemme, P. Beltrao, M. Vignuzzi, A. García-Sastre, K.M. Shokat, B.K. Shoichet, N.J. Krogan, A SARS-CoV-2 protein interaction map reveals targets for drug repurposing, Nature 583 (7816) (2020) 459–468.
[90] C.A. Birch, O. Molinar-Inglis, J. Trejo, Subcellular hot spots of GPCR signaling promote vascular inflammation, Curr. Opin. Endocr. Metab. Res. 16 (2021) 37–42.
[91] K.K. Singh, G. Chaubey, J.Y. Chen, P. Suravajhala, Decoding SARS-CoV-2 hijacking of host mitochondria in COVID-19 pathogenesis, Am. J. Physiol. Physiol. 319 (2) (2020) C258–C267.
[92] A. Pilotto, S. Masciocchi, I. Volonghi, E. del Zotto, E. Magni, V. De Giuli, F. Caprioli, N. Rifino, M. Sessa, M. Gennuso, The clinical spectrum of encephalitis in COVID-19 disease: the ENCOVID multicentre study, Medrxiv (2020).
[93] R. Guo, M. Xiao, W. Zhao, S. Zhou, Y. Hu, M. Liao, S. Wang, X. Yang, R. Chai, M. Tang, 2D Ti3C2TxMXene couples electrical stimulation to promote proliferation and neural differentiation of neural stem cells, Acta Biomater. 139 (2022) 105–117.
[94] J. Xie, X. Li, Y. Xia, Putting electrospun nanofibers to work for biomedical research, Macromol. Rapid Commun. 29 (22) (2008) 1775–1792.
[95] I. Bružauskaitė, D. Bironaitė, E. Bagdonas, E. Bernotienė, Scaffolds and cells for tissue regeneration: different scaffold pore sizes—different cell effects, Cytotechnology 68 (2016) 355–369.
[96] Y. Zhang, Y. Yan, H. Qiu, Z. Ma, K. Ruan, J. Gu, A mini-review of MXene porous films: preparation, mechanism and application, J. Mater. Sci. Technol. 103 (2022) 42–49.
[97] T.M. Rawson, L.S.P. Moore, N. Zhu, N. Ranganathan, K. Skolimowska, M. Gilchrist, G. Satta, G. Cooke, A. Holmes, Bacterial and fungal coinfection in individuals with coronavirus: a rapid review to support COVID-19 antimicrobial prescribing, Clin. Infect. Dis. 71 (2020) 2459–2468.
[98] G.P. Lim, C.F. Soon, M. Morsin, M.K. Ahmad, N. Nayan, K.S. Tee, Synthesis, characterization and antifungal property of Ti3C2Tx MXene nanosheets, Ceram. Int. 46 (12) (2020) 20306–20312.
[99] A. Arabi Shamsabadi, M. Sharifian Gh., B. Anasori, M. Soroush, Antimicrobial mode-of-action of colloidal Ti3C2Tx MXene nanosheets, ACS Sustain, Chem. Eng. 6 (12) (2018) 16586–16596.
[100] H. Huang, R. Jiang, Y. Feng, H. Ouyang, N. Zhou, X. Zhang, Y. Wei, Recent development and prospects of surface modification and biomedical applications of MXenes, Nanoscale 12 (3) (2020) 1325–1338.
[101] Y. Liu, Q. Han, W. Yang, X. Gan, Y. Yang, K. Xie, L. Xie, Y. Deng, Two-dimensional MXene/cobalt nanowire heterojunction for controlled drug delivery and chemo-photothermal therapy, Mater. Sci. Eng. C. 116 (2020), 111212.
[102] Z. Xia, Q. Huang, S. Guo, Recent progress on synthesis, structure and electrocatalytic applications of MXenes, FlatChem 17 (2019), 100129.
[103] A. VahidMohammadi, J. Rosen, Y. Gogotsi, The world of two-dimensional carbides and nitrides (MXenes), Science 372 (6547) (2021).
[104] Z. Wu, J. Shi, P. Song, J. Li, S. Cao, Chitosan/hyaluronic acid based hollow microcapsules equipped with MXene/gold nanorods for synergistically enhanced near infrared responsive drug delivery, Int. J. Biol. Macromol. 183 (2021) 870–879.
[105] Q.M. Sajid Jamal, A.H. Alharbi, V. Ahmad, Identification of doxorubicin as a potential therapeutic against SARS-CoV-2 (COVID-19) protease: a molecular docking and dynamics simulation studies, J. Biomol. Struct. Dyn. (2021) 1–15.
[106] S. Naicker, C.-W. Yang, S.-J. Hwang, B.-C. Liu, J.-H. Chen, V. Jha, The novel coronavirus 2019 epidemic and kidneys, Kidney Int. 97 (2020) 824–828.
[107] F. Meng, M. Seredych, C. Chen, V. Gura, S. Mikhalovsky, S. Sandeman, G. Ingavle, T. Ozulumba, L. Miao, B. Anasori, MXene sorbents for removal of urea from dialysate: a step toward the wearable artificial kidney, ACS Nano 12 (2018) 10518–10528.
[108] Y. Wang, W. Feng, Y.u. Chen, Chemistry of two-dimensional MXene nanosheets in theranostic nanomedicine, Chinese Chem. Lett. 31 (4) (2020) 937–946.
[109] K.A.L. Shareef, M. Bakouri, Cytokine blood filtration responses in COVID-19, Blood Purif. 50 (2021) 141–149.
[110] V. Presser, S.-H. Yeon, C. Vakifahmetoglu, C.A. Howell, S.R. Sandeman, P. Colombo, S. Mikhalovsky, Y. Gogotsi, Hierarchical porous carbide-derived carbons for the removal of cytokines from blood plasma, Adv. Healthc. Mater. 1 (6) (2012) 796–800.
[111] J. Liu, X. Jiang, R. Zhang, Y. Zhang, L. Wu, W. Lu, J. Li, Y. Li, H. Zhang, MXene-enabled electrochemical microfluidic biosensor: applications toward multicomponent continuous monitoring in whole blood, Adv. Funct. Mater. 29 (2019) 1807326.
[112] N. Dwivedi, C. Dhand, P. Kumar, A.K. Srivastava, Emergent 2D materials for combating infectious diseases: the potential of MXenes and MXene–graphene composites to fight against pandemics, Mater. Adv. 2 (2021) 2892–2905.
[113] M. Serhani, H. Labbardi, Mathematical modeling of COVID-19 spreading with asymptomatic infected and interacting peoples, J. Appl. Math. Comput. 66 (1-2) (2021) 1–20.
[114] M. Muenchhoff, H. Mairhofer, H. Nitschko, N. Grzimek-Koschewa, D. Hoffmann, A. Berger, H. Rabenau, M. Widera, N. Ackermann, R. Konrad, Multicentre comparison of quantitative PCR-based assays to detect SARS-CoV-2, Germany, March 2020, Eurosurveillance 25 (2020) 2001057.

[115] W.Y. Chen, H. Lin, A.K. Barui, A.M.U. Gomez, M.K. Wendt, L.A. Stanciu, DNA-Functionalized Ti3C2T x MXenes for selective and rapid detection of SARS-CoV-2 nucleocapsid gene, ACS Appl. Nano Mater. 5 (2) (2022) 1902–1910.
[116] A. Kumar, A. Arora, P. Sharma, S.A. Anikhindi, N. Bansal, V. Singla, S. Khare, A. Srivastava, Is diabetes mellitus associated with mortality and severity of COVID-19? A meta-analysis, Diabetes Metab. Syndr. Clin. Res. Rev. 14 (4) (2020) 535–545.
[117] P.K. Kalambate, N.S. Gadhari, X. Li, Z. Rao, S.T. Navale, Y. Shen, V.R. Patil, Y. Huang, Recent advances in MXene–based electrochemical sensors and biosensors, TrAC Trends Anal. Chem. 120 (2019), 115643.
[118] R.B. Rakhi, P. Nayak, C. Xia, H.N. Alshareef, Novel amperometric glucose biosensor based on MXene nanocomposite, Sci. Rep. 6 (2016) 1–10.
[119] Y. Lei, W. Zhao, Y. Zhang, Q. Jiang, J. He, A.J. Baeumner, O.S. Wolfbeis, Z. L. Wang, K.N. Salama, H.N. Alshareef, A MXene-based wearable biosensor system for high-performance in vitro perspiration analysis, Small 15 (2019) 1901190.
[120] E. Redondo, M. Pumera, MXene-functionalised 3D-printed electrodes for electrochemical capacitors, Electrochem. Commun. 124 (2021), 106920.
[121] S. Shirazi, S. Mami, N. Mohtadi, A. Ghaysouri, H. Tavan, A. Nazari, T. Kokhazadeh, R. Mollazadeh, Sudden cardiac death in COVID-19 patients, a report of three cases, Future Cardiol. 17 (1) (2021) 113–118.
[122] R. Yang, F. Li, W. Zhang, W. Shen, D.i. Yang, Z. Bian, H. Cui, Chemiluminescence immunoassays for simultaneous detection of three heart disease biomarkers using magnetic carbon composites and three-dimensional microfluidic paper-based device, Anal. Chem. 91 (20) (2019) 13006–13013.
[123] X. Mi, H. Li, R. Tan, B. Feng, Y. Tu, The TDs/aptamer cTnI biosensors based on HCR and Au/Ti3C2-MXene amplification for screening serious patient in COVID-19 pandemic, Biosens. Bioelectron. 192 (2021), 113482.
[124] X. Peng, Y. Zhang, D. Lu, Y. Guo, S. Guo, Ultrathin Ti3C2 nanosheets based “off-on” fluorescent nanoprobe for rapid and sensitive detection of HPV infection, Sens. Actuators B Chem. 286 (2019) 222–229.
[125] Z. Lin, J.i. Liu, W. Peng, Y. Zhu, Y. Zhao, K. Jiang, M. Peng, Y. Tan, Highly stable 3D Ti3C2T x MXene-based foam architectures toward high-performance terahertz radiation shielding, ACS Nano 14 (2) (2020) 2109–2117.
[126] K. O’Dowd, K.M. Nair, P. Forouzandeh, S. Mathew, J. Grant, R. Moran, J. Bartlett, J. Bird, S.C. Pillai, Face masks and respirators in the fight against the COVID-19 pandemic: a review of current materials, advances and future perspectives, Materials (Basel) 13 (2020) 3363.
[127] M. Yanes-Lane, N. Winters, F. Fregonese, M. Bastos, S. Perlman-Arrow, J. R. Campbell, D. Menzies, R. Serra, Proportion of asymptomatic infection among COVID-19 positive persons and their transmission potential: a systematic review and meta-analysis, PLoS One 15 (11) (2020) e0241536.
[128] S. Lee, E.H. Kim, S. Yu, H. Kim, C. Park, S.W. Lee, H. Han, W. Jin, K. Lee, C.E. Lee, J. Jang, C.M. Koo, C. Park, Polymer-laminated Ti3C2TX MXene electrodes for transparent and flexible field-driven electronics, ACS Nano 15 (5) (2021) 8940–8952.
[129] W. Yang, J. Yang, J.J. Byun, F.P. Moissinac, J. Xu, S.J. Haigh, M. Domingos, M. A. Bissett, R.A.W. Dryfe, S. Barg, 3D printing of freestanding MXene architectures for current-collector-free supercapacitors, Adv. Mater. 31 (2019) 1902725.